




# Thin-walled aluminium waste remelting in circulation circuit with magnetodynamic pump

Oleksiy Smirnov<sup>1</sup>, Vladyslav Fikssen<sup>1</sup>, Volodymyr Kukhar<sup>2</sup>, Maksym Goryuk<sup>1</sup>, Oleksandr Hrushko<sup>3,\*</sup> , Oleksandr Rud<sup>4</sup>, and Viktor Lomakin<sup>5</sup>

<sup>1</sup> Department of Magnetohydrodynamics, Physico-Technological Institute of Metals and Alloys, National Academy of Sciences of Ukraine, Kyiv 03142, Ukraine

<sup>2</sup> Department of Metallurgy, Material Science and Production Organization, Technical University "Metinvest Polytechnic", LLC, Zaporizhzhia 69008, Ukraine

<sup>3</sup> Department for Integrated Sensor Systems, University for Continuing Education Krems (Danube University Krems), 2700 Wiener Neustadt, Austria

<sup>4</sup> Department of Structure and Properties of Solid Solutions, G.V. Kurdyumov Institute for Metal Physics, National Academy of Sciences of Ukraine, Kyiv 03142, Ukraine

<sup>5</sup> Department of Material Science and Foundry, Mechanical and Technological Faculty, Central Ukrainian National Technical University, Kropyvnytskyi 25006, Ukraine

**Received:** 14 April 2024

**Accepted:** 26 July 2024

© The Author(s), 2024

## ABSTRACT

Modern technologies for remelting thin-walled aluminium waste are considered, and a new method to implement such process is proposed. This made it possible to increase the yield of a suitable remelted product to 83% from the mass of the initial remelting portion. The main idea is to use indirect heating of the charge. This will allow to significantly reduce the irreversible loss of metal due to burning which can reach 60%. In the proposed process, solid waste is melted by overheated melt stream. The movement of such stream is provided by the action of electromagnetic field. For the practical implementation of the offered idea, there was used a magnetodynamic pump (MDP) designed in the Physico-Technological Institute of Metals and Alloys of National Academy of Sciences of Ukraine. The MDP has a significantly higher heat and power factor than electromagnetic pumps of travelling magnetic field which are often used in similar technologies. Mathematical model of the remelting process of aluminium thin-walled and fine charge due to convective heat transfer was developed. On the basis of this model, an engineering calculation of the specific process of remelting used aluminium cans in the liquid aluminium stream was also carried out. The obtained results were used at further conducting a full-scale experiment. There is designed and successfully practically tested the experimental two-chamber circulation circuit with MDP for remelting thin-walled aluminium waste. Recommendations for further development of the proposed process were formulated.

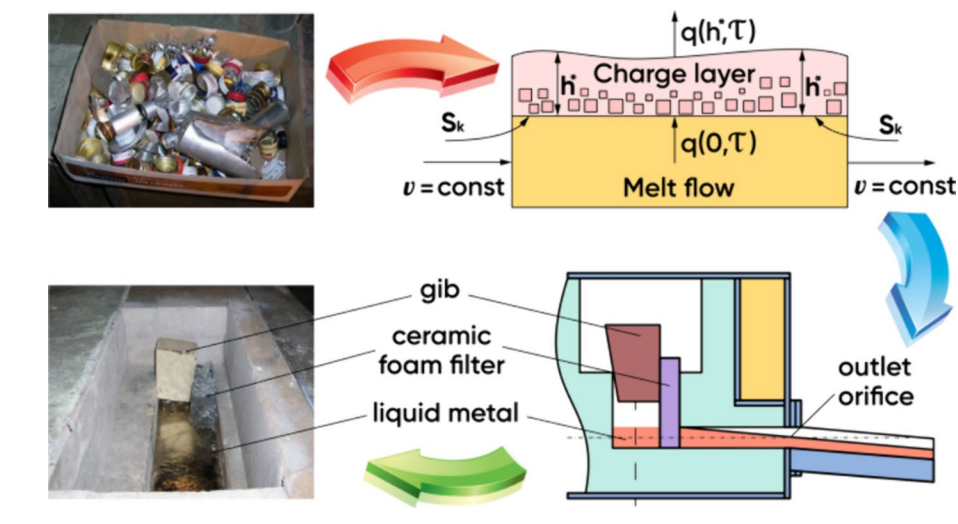
Handling Editor: M. Grant Norton.

Address correspondence to E-mail: Oleksandr.Hrushko@donau-uni.ac.at

<https://doi.org/10.1007/s10853-024-10062-3>

Published online: 21 August 2024

## GRAPHICAL ABSTRACT



## Introduction

Aluminium-based alloys are increasingly used in construction, energy, transport, aviation, etc. Paper [1] outlines the advantages of using aluminium in the automotive, construction, aerospace industries, etc., and indicates the prospects for increasing the consumption of aluminium scrap for the re-production of aluminium alloys. The largest number of products made of aluminium and its alloys is found in mechanical engineering ( $\sim 45\%$ ). Construction is in the second place in terms of aluminium consumption ( $\sim 30\%$ , respectively). A significant amount of aluminium is consumed in the manufacture of various types of packaging ( $\sim 20\%$ ), in energy sector and at electricity transportation [2]. Recently, the share of aluminium alloys in the production of household and food containers, in particular, beverage cans, food foil, coffee capsules, etc., has been constantly increasing [3].

The rapidly increasing shortage of primary non-ferrous metals and the need to ensure high competitiveness by reducing the cost of cast products make research aimed at technologies for deeper processing and increasing the share of metal waste as a raw material in metallurgical and foundry production [4]. However, the widespread use of scrap at metallurgical enterprises, as well as cast products obtained from secondary alloys, is by the shortcomings of existing technologies for their processing and further involvement in production [5].

Meanwhile, metallurgy of secondary aluminium allows for significant savings in raw materials and energy. Recycling technology makes it possible to reduce the depletion of subsoil assets, minimize harmful emissions into the atmosphere, and reduce the accumulation of waste aluminium industrial and household products. Herewith, the energy costs for the production of 1 tonne of secondary aluminium (approximately 0.7–0.8 MWh) are only 5% of the costs for the production of 1 tonne of primary aluminium (15–16 MWh) [6]. The economic and environmental benefits of remelting aluminium, which does not lose its properties during recycling, as well as the value of aluminium scrap, are noted in [4, 7], which discusses the need for sorting, pressing, or shredding aluminium cans before remelting. Aluminium recycling saves up to 95% of the energy required to produce primary metal, as aluminium recycling requires only 5% of the energy to produce secondary metal compared to primary metal and generates only 5% of greenhouse gas emissions [7]. The study [8] also emphasizes that aluminium recycling has a number of key environmental and economic benefits. However, the presence of problematic impurities in aluminium should be taken into account, which negatively affect the energy costs of melting: Si, Mg, Ni, Zn, Pb, Cr, Fe, Cu, V, and Mn. It is pointed out that it is necessary to identify strategies for the entire production cycle to reduce the accumulation of such elements. The concentration of alloying elements during recycling can lead to the production of secondary metals and alloys that do not

meet specifications, and it was predicted that in 2050, Japan, USA, Europe, and China will accumulate about 12 400 thousand tonnes of obsolete scrap, which will be difficult to recycle due to the high concentration of alloying elements [9].

In addition, the production of one metric tonne of primary aluminium requires about four metric tonnes of bauxite and produces about two metric tonnes of red mud. Bauxite mining is also an activity that causes environmental problems. Paper [10] notes that bauxite, as a raw material for aluminium, is rare on earth, and the area and amount of aluminium use are increasing over time. The authors [10] present a technology for recycling aluminium from waste and scrap by remelting in an induction furnace, casting into small ingots, and hardening to the parameters of 7075 aluminium alloy. Accordingly, the favourable energy balance makes aluminium an excellent product for recycling, since the main component in the cost of primary aluminium production is electricity. Therefore, aluminium has another significant advantage: Its waste has a higher market value than many other materials [6].

Recycled aluminium waste in the metal circulation system has a different initial origin: cast, heat-treated, deformed, and many options of combined treatments. For example, [11] developed a technology for processing a mixture of aircraft aluminium scrap into a 7075 alloy that meets the requirements of GB/T 3190-2008. The technology includes melting aluminium scrap, adjusting the composition, refining, and casting into ingots, followed by extrusion and heat treatment. As a result of the processing, the mechanical properties of all Al profiles exceeded the requirements of ASTM B209-14 and B221M-13. The heat-treated bars had the highest tensile strength (591 MPa), yield strength (534 MPa), elongation (10.0%), and stress-corrosion susceptibility factor (44.8) [11]. The processing of aircraft aluminium scrap by smelting, extrusion, and heat treatment is also described in [12]. Researchers [13] studied the effect of the type of recycled aluminium waste on the impact strength and hardness, as well as the microstructure, during the melting process. It was shown that the hardness and impact strength of aluminium obtained from melting down beverage cans are an average between the properties of aluminium obtained from a petrol engine piston and an aluminium pan. The paper [14] shows that the addition of zinc (Zn) and copper (Cu) in the form of alloying elements improves the mechanical properties of recycled sand cast Al–Cu–Zn alloys. The paper [15] reports the

results of strontium Sr modification of a cast Al–Si secondary alloy. It was found that an increase in the amount of Sr increases the impact strength and changes the morphology of eutectic silicon, which affects the fracture surface. Study [16] found that the highest fluidity and tensile strength of the Al–Si alloy were obtained by gravity casting with the addition of 0.4% wt% sodium-based flux at 740 °C. The range of target properties of aluminium alloys obtained using recycled aluminium may include the use of materials with the effect of shape memory [17] or superplastic forming [18].

In [19], researchers focused on the use of secondary aluminium in the automotive industry to reduce the consumption of primary aluminium. It is noted that secondary aluminium alloys have the same microstructural parameters and properties as primary aluminium alloys. The study [20] provided a comprehensive, industry-wide analysis of aluminium reuse and recycling in the most energy-efficient way in the automotive, aircraft, packaging, and construction industries, electrical and mechanical engineering equipment manufacturing, etc. New technologies for processing automotive scrap are discussed in [4]. The advantages of laser-induced breakdown spectroscopy (LIBS) and solid-state processing (with preliminary compression and extrusion at room or moderate temperature) are highlighted in terms of achieving higher material yields compared to conventional melting. Paper [21] describes a method of modifying aluminium alloys to produce materials for the manufacture of aircraft and automotive engine housings and parts.

The issue of the recycling yield (reduction of unavoidable losses) for aluminium is addressed in [22]. The study found that when recycling aluminium waste, more non-metallic contaminants and a higher ratio of surface area to body volume result in a lower metal yield (cast ingots produced better results than rolling cuts under similar conditions; bottle caps are easier to recycle than foil [22]). At the same time, the composition of the salt flux has a greater impact on recycling efficiency than the temperature factor. Articles [21, 23] indicate that the presence of toxic (cadmium) and expensive (silver) strengthening additives significantly limits the potential for recycling aluminium alloys. The influence of casting parameters on the efficiency of aluminium beverage cans recycling using an electric induction furnace was investigated in [24]. In this case, the cans were pre-compacted into “packages” (pressed), and during remelting, the bath

temperature and the amount of flux were varied. After pouring into moulds, the degree of recovery of aluminium by mass was determined, and it was determined that bath temperatures above 750 °C and flux amounts of at least 10 wt.% lead to good recovery of aluminium after the recycling of cans [24].

In [9], a multimaterial dynamic pinch analysis of the aluminium flow in developed countries (Japan, USA, Europe, and China) was carried out, for which 60, 65, 30, and 85% of the potential for reducing primary aluminium consumption from the current level was established, respectively. Paper [25] shows the relevance of separating aluminium scrap streams and the industry's dependence on the secondary aluminium market, including the volume of aluminium beverage cans recycled. Kevorkijan V. [26] pointed out that a significant portion of secondary aluminium scrap is used to produce relatively cheaper casting alloys, losing a significant portion of their potential added value. Design algorithms for increasing the share of recycled scrap were developed in [26]. The algorithms include two ways: (a) applying pre-sorting of scrap into fractions with the required chemical composition and mixing them to obtain wrought alloys with predictable composition and properties; or (b) expanding the tolerance limits for the content of alloying elements (which requires radical changes in existing standards) and creating non-standard "recycling-friendly" alloys.

As a result of technological treatments, all recycled metals have a completely characteristic structural state and different heredity, which can have a significant impact on the quality of cast products (pig alloys, ingots, castings, granules, etc.) obtained from recycled materials. In most cases, scrap is used to produce cast alloys for the automotive or aerospace industries. In addition, most recycling plants are located near the automotive industry. Improving the quality of cast products is the most important task of metallurgical and foundry industries. At present stage, relevant interrelated directions are reducing the mass of castings and increasing the share of castings from light alloys (for example, from alloys based on aluminium and magnesium). Herewith, aluminium recycling requires new technological approaches and solutions. Thus, a special place in practice is occupied by the problem of recycling thin-walled aluminium products that have a loss rate of 30–40% and more [5]. For example, paper [27] developed a methodology for the recycling of aluminium cans together with primary aluminium when the product is converted into

laminated electrically conductive tape for industrial applications. The article [28] also contains information on the technology of recycling used aluminium beverage cans (UBCs) and experimentally shows that the high manganese content and susceptibility to oxidation reduce the efficiency of can recycling. At the initial stages of recycling, cans are pressed or shredded, and there are several effective methods of cutting (shredding) [29, 30].

Currently, the leading manufacturers have developed a whole arsenal of chemical and physical methods for influencing charge metals and alloys in the "solid–liquid–solid state" system, which are used in the production of cast products from primary metals and for critical alloys. However, in secondary metallurgy, these processes are used to an extremely limited extent. The paper [31] shows the possibility of using ultrafast laser radiation (laser energy) to melt thin aluminium plates. The selective laser melting method was used to develop thin-walled AlSi<sub>10</sub>Mg alloy parts [32], and the effect of target thickness on product dimensional distortion was investigated. For thinner walls, maximum distortions and deviations from the design thickness were observed. To reduce the burning of cans during heating before melting, they are briquetted and extruded [33], and during remelting, the melt is fluxed [28]. Paper [34] investigates the transformation of AA6060 aluminium alloy chips into finished products by hot extrusion followed by cold extrusion. In this case, the quality of finished parts based on chips significantly depends on the adhesion strength between individual chips, which is established during hot extrusion. In the work [35], the authors found that for compression conditions of aluminium cans, characteristic of pressing, extruding, and briquetting, the wall thickness of the can as well as the varnish coating thickness affect the strength characteristics of processes, which must be taken into account both when designing cans and when recycling them. In addition, the energy-force modes of deformation of cans are influenced by storage conditions (and the associated ageing processes of aluminium alloys), as well as climatic conditions [36].

Paper [37] shows that in the manufacture and subsequent processing of thin-walled aluminium products, the quality of their surface deteriorates with an increase in the concentration of aluminium carbide particles formed during the production of primary aluminium. At the same time, the carbide concentration decreases rapidly during remelting, and this

decrease occurs faster in air than in argon. Therefore, recycled secondary aluminium can replace the secondary one with exceptionally high profit margins, but it is necessary to develop technological solutions that allow us to control the process of obtaining the final properties of aluminium products.

Figure 1 shows some of the most common types of households thin-walled aluminium waste—drink containers, packaging tape, foil, etc. The efficiency of remelting such aluminium waste directly depends on the method of transferring thermal energy to the object being remelted and is determined by parameters such as aluminium loss (Al-yield) and recycling yield [38].

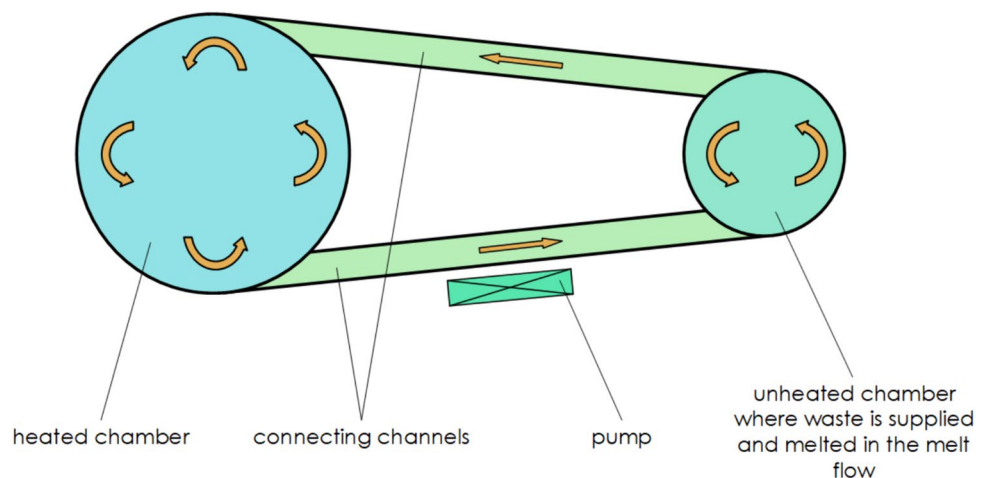
In case of direct heating, irreversible losses of melted thin-walled and small scrap by weight (actually loss) can reach 50–60% [5]. The results of [38] also show that cans recycling with drossing flux provides 55.2 to 59.1% recycling yield, and recycling without flux provides 52.5 to 54.7% recycling yield. One of the ways to reduce such losses is to eliminate direct heating of such a charge, especially in case of using a gas burner in a furnace unit where

temperature control is carried out. At the same time, a controlled temperature regime is formed to ensure the quality of the technological process [39]. Better results, both in terms of reducing aluminium and alloy losses and producing high-purity melts, are achieved when remelting in induction furnaces using cold crucible or skull melting technologies [40–42]. In addition to increasing the yield of usable aluminium, an urgent problem in the recycling of used aluminium beverage cans is the removal of organic residual contaminants, lacquer, and paint coatings [43–45]. For such firing and thermal de-coating, pre-treatment is used in two-chamber [43, 46, 47] or multi-chamber [44, 45] furnaces, which have a much wider range of functions. It is most rational to melt a thin-walled and small charge in a stream of superheated melt [21, 48]. Therefore, modern technologies of remelting thin-walled aluminium waste are usually based on the use of two-chamber systems connected by channels, on one of which a pump is installed to ensure circulation of the melt in the system [43, 49] (Fig. 2).

**Figure 1** Remelted waste of thin-walled aluminium charge with a developed surface (for example, cans for various drinks).



**Figure 2** Flowchart of the system for remelting aluminium waste (arrows indicate the direction of the melt movement and mixing).



One of the chambers is heated by a heat source and serves to accumulate the melt, the other, as a rule, is unheated and is intended for remelting the charge in the melt flow coming from the heated chamber. "Sometimes the second chamber provides additional heating of the melt in order to compensate for its heat loss during circulation and remelting of the charge, and therefore is an induction crucible furnace [43, 49]. In some cases the entire melting system is structurally designed and functions as an induction channel device with a horizontally located channel [43, 50]. Herewith, the circulation of metal in such a system is almost throughout carried out using a pump installed on one of the connecting channels (as of today, most often a linear electromagnetic pump or a running magnetic field pump), which is able to provide high values of process productivity due to the ability to develop high mass flow rates when pumping the melt [21, 48, 51, 52].

As mentioned above, modification with alloying additives is not always energy efficient and complicates aluminium processing. Ultrasonic processing is known to refine the microstructure of a cast alloy, and it was found [53] that in the presence of iron impurities, the grinding of Al grains is more intense. To suppress and prevent defects, technological methods of creating dynamic effects during casting and solidification of alumina are becoming widespread [48]. High efficiency of dynamic influence is achieved due to the simultaneous influence of vibroimpulses and regulated forced stirring on the melt. The study [48] is based on the idea of using the phenomenon of the linear pinch-effect to influence its thermal and force factors on the aluminium melt during its multiple circulating pumps through a local zone with reduced pressure relative to atmospheric pressure. In [21], it was proposed to use the energy of electromagnetic fields and magnetohydrodynamic (MHD) effects to treat alloys in the liquid state. The study showed that the developed MHD treatment of alloys ensures the crushing of the structure and an increase in the main mechanical properties of aluminium alloys in the solid state, which is actually their physical modification with the exclusion of the use of strengthening additives.

Thus, it is necessary to highlight the scientific achievements, which are the focus of the research in this article:

- Improvement of the strategy to increase the share of waste aluminium as a raw material in metallurgi-

cal and foundry production, including for the creation of non-standard alloys;

- Recycling of hard-to-dispose of used aluminium cans as thin-walled bodies, the melting of which in traditional melting units is difficult; increasing the efficiency of recycling and Al-yield (reduction of metal losses) in the remelting of thin-walled aluminium products;

- Reducing the influence of impurities in aluminium on energy costs during remelting and increasing the purity of alloys, conditioned for further use;

Physical modification of the melt by magnetodynamic methods instead of modification with the addition of alloying elements, while ensuring high productivity; revealing the peculiarities of changes in the chemical composition of the experimental alloy during remelting; development of the effect of temperature removal of residual organic contaminants and paint coatings in the jet of superheated melt driven by a circulation pump;

- Increasing the efficiency of electromagnetic field energy and magnetohydrodynamic (MHD) effects on the mixed-melt by using magnetodynamic pump to pump the melt through a local zone with reduced pressure; determination of the most preferable speed mode of melt circulation, overpressure for metal lifting and power of magnetodynamic pump;
- Development of the mathematical model describing the charge heating by the jet of heated melt on the contact surface and kinetics of its melting in conditions of convective heat transfer with determination of rational technological modes at the given productivity of remelting process; improvement of the method of calculation of heat energy transfer to the remelted raw material.

## Materials and methods

### Features of the method

The paper proposes an experimental device for remelting thin-walled aluminium waste, which completely preserves the principle of operation and the main elements of the flowchart discussed above (see Fig. 2). The main distinctive feature is the use of a magnetodynamic pump (MDP) designed by Physico-Technological Institute of Metals and Alloys (PTIMA) National Academy of Sciences (NAS) of Ukraine [54–56].

Magnetodynamic pumps provide transportation of liquid metal through closed pipelines and compensation for heat loss of the melt. The general arrangement and principle of operation of such a device can be demonstrated using the example of the MDP-3 pump (Fig. 3).

Voltage is applied to the windings of the inductor and the electromagnet. In the working area, there is interaction of the inductor-induced electric current  $I_C$  in the liquid metal located in the induction channel with the external magnetic field  $\Phi$  created by the electromagnet. As a result of such interaction and in accordance with the left-hand rule, an electromagnetic force  $F$  is generated, ensuring the movement of the liquid metal at a certain speed  $v$ . In this case,

the movement of the melt can be organized both in a closed circuit and during transportation (pouring) of liquid metal into a casting mould, crystallizer, or ladle.

A laboratory magnetohydrodynamic (MHD) circulation circuit (Fig. 4) is proposed for remelting waste aluminium alloys, which incorporates a magnetodynamic pump (MDP) designed by PTIMA NAS of Ukraine [54–56]. Compared to a circuit with linear electromagnetic pumps and pumps of travelling magnetic field pumps, MDP in this case provides the following main advantages: (1) higher electric power factor, amounting to 0.6–0.7 versus 0.2–0.3; (2) compensation for heat loss of the melt and the possibility of its additional heating during transportation with high thermal efficiency (up to 0.9); (3) possibility of

**Figure 3** MDP-3 magnetodynamic pump and creation of electromagnetic force in the melt.

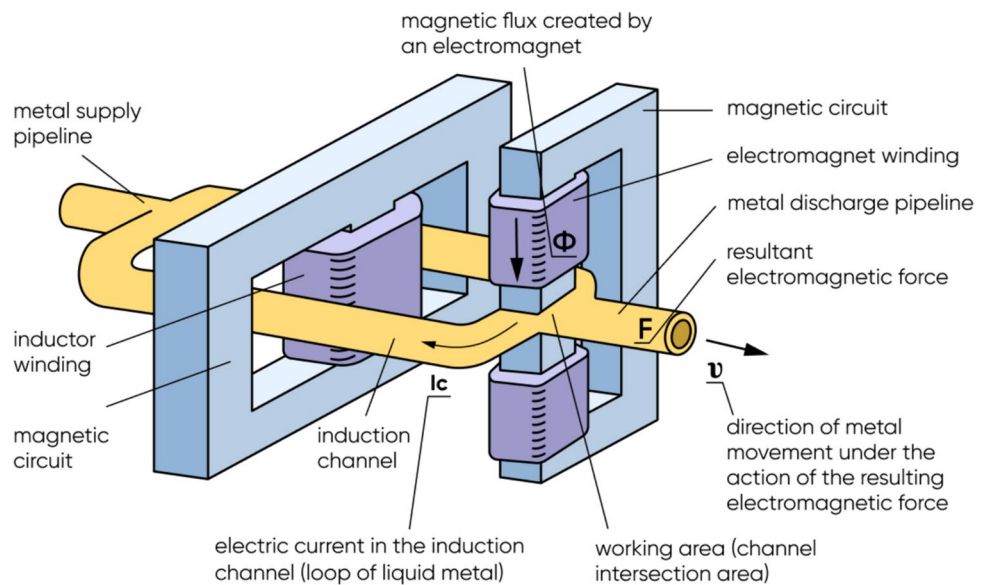
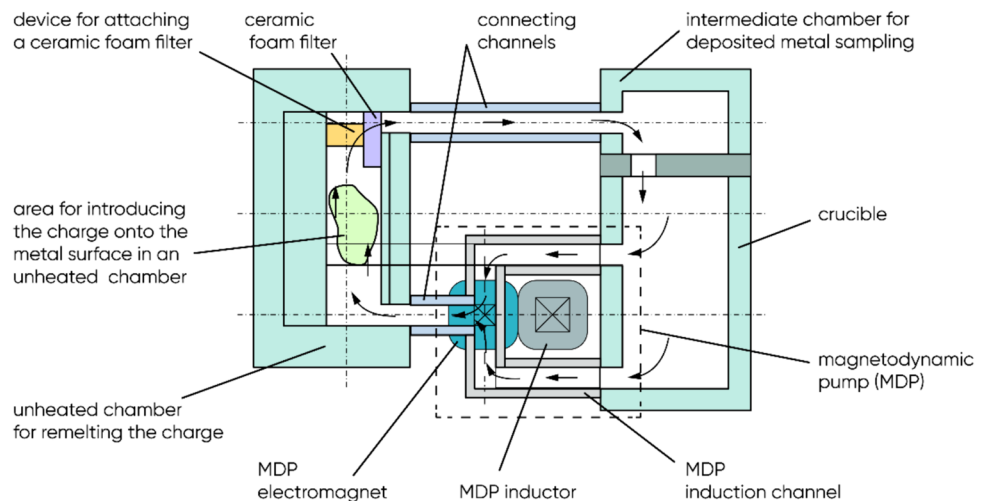


**Figure 4** Scheme of the MHD circulation circuit for remelting aluminium waste (arrows indicate the direction of circulation of liquid metal in the system).



melting metal that has hardened after a sudden (emergency) power outage; and (4) convenience of out-of-furnace processing and filtration of molten metal, etc.

The latter is especially important in the light of the fact that the melted thin-walled and small aluminium waste is heavily contaminated with various substances of technical and household origin (paints, varnishes, oils, food residues, etc.). In addition, during the remelting process, additional contamination of the liquid metal with gases and non-metallic inclusions is possible due to contact with the furnace atmosphere and refractory materials. All this leads to environmental deterioration in production, the formation of a large amount of dross on the surface of the melt and the need to apply special measures both when preparing waste for remelting and during refining processing of the obtained melt [2, 11, 45, 57–60]. The use of MDP in the proposed scheme will make it possible to organize effective refining of the melt from gases and inclusions—for example, using refining gas and flux media and ceramic foam

filters, as well as due to purely physical influences, in particular, electromagnetic and MHD effects as a controlled local pinch effect [36].

### Equipment and operation modes

According to the scheme presented in Fig. 4, an experimental laboratory MHD circulation circuit (Fig. 5) was assembled for remelting thin-walled aluminium waste.

The circuit has the following elements connected in series:

- Heated chamber (using nichrome spirals);
- Magnetodynamic pump, MDP-3A type;
- Unheated melting chamber;
- Channel (gutter) through which the melt returns to the heated chamber.

The technical parameters of laboratory circuit are given in Table 1.

**Figure 5** External view of the experimental MHD circulation melting circuit.

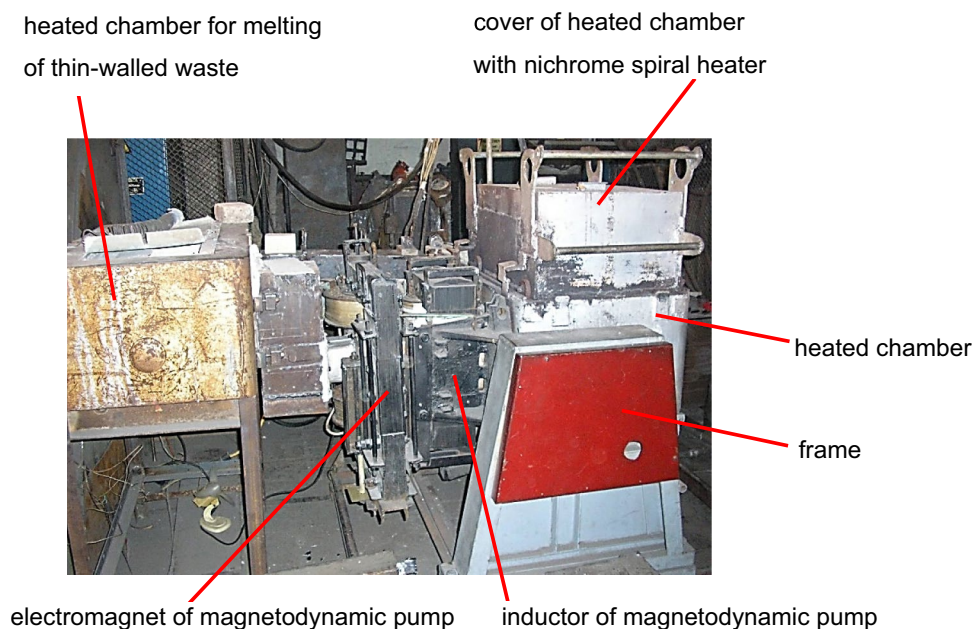


**Table 1** Technical parameters of experimental circuit for melting of thin-walled aluminium waste

Parameter	Value
Electric power of nichrome spiral in the heated chamber, kW	8
Total electric power of magnetodynamic pump MDP-3A, kW	14
Inductor & electromagnet voltage range, V	0–380
Capacity of the circuit by aluminium melt, kg	100
Overall dimensions (length × wideness × height), mm	1950 × 1750 × 1300



## Results

### Mathematical model

The study and determination of rational parameters for the melting process of aluminium scrap in a flow-through unheated chamber of the developed MHD circulation circuit with MDP are associated with significant difficulties. The need to vary a large number of factors influencing the kinetics of melting of the charge under conditions of convective heat transfer makes the process of experimental research cumbersome. The task of determining rational technological regimes with a given process productivity is extremely difficult. All this makes it advisable and even necessary to use mathematical modelling methods to study the melting process.

As already noted, aluminium chips and other types of aluminium scrap metal are characterized by a very small thickness  $l$  (about  $10^{-4}$ – $10^{-3}$  m) and a relatively large surface. Obviously, with such small thicknesses, the inhomogeneity of the temperature fields of bodies heated in the melting chamber of the unit by the melt flow should be small.

However, the value of the heat transfer coefficient by convection  $\alpha$  during heat exchange between a flow of overheated melt and a heated solid object is unknown and depends mainly on the thermophysical characteristics of the solid body material, the melting alloy, as well as on the temperature and speed of the latter.

The process of heating to the melting point of a single body in the form of a metal plate placed on the free surface of the melt flow in the melting chamber was considered (Fig. 6).

Here:  $v$ —melt flow speed, m/s;  $F$ —contact area of the stationary plate with the melt flow,  $m^2$ ;  $q(0, \tau)$  and  $q(l, \tau)$ —heat flux density, respectively, at the boundaries at  $x = 0$  and  $x = l$ ,  $W/m^2$ .

Such a plate can be represented as an infinite body through which heat is transferred only in the direction  $x$ .

The differential equation of thermal conductivity for such a heated plate has the form of [61, 62]:

$$c_T \rho_T \frac{\partial T}{\partial \tau} = \lambda_T \frac{\partial^2 T}{\partial x^2}, \tau > 0, 0 < x < l \quad (1)$$

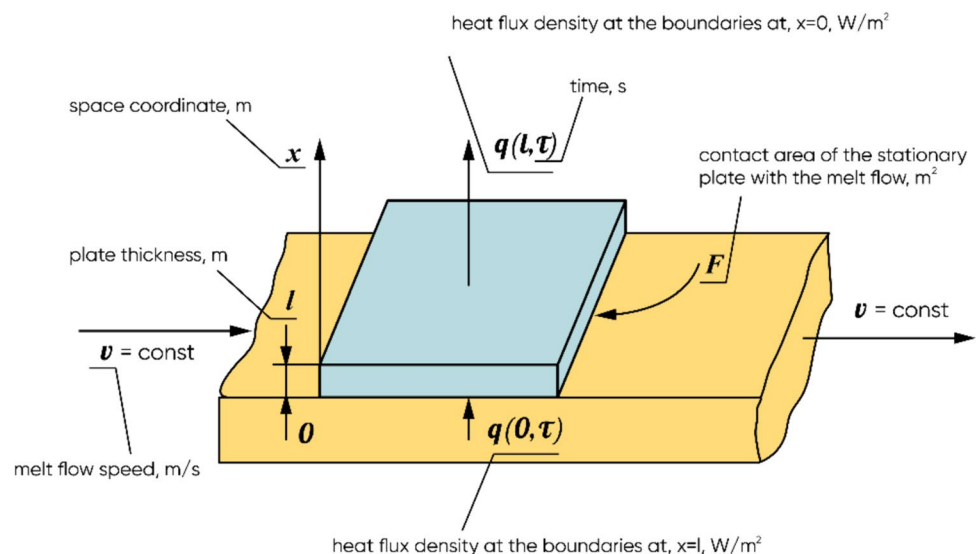
where  $c_T$ —heat capacity of aluminium plate,  $J/(kg \cdot K)$ ;  $\rho_T$ —aluminium plate density,  $kg/m^3$ ;  $T$ —plate temperature,  $K$ ;  $\tau$ —time,  $s$ ;  $\lambda_T$ —thermal conductivity coefficient of the material of the heated solid body,  $W/(m \cdot K)$ ;  $x$ —space coordinate,  $m$ ;  $l$ —plate thickness,  $m$ .

Extending Eq. (1) to the whole area  $x \in [0, l]$ ; then

$$\int_0^l c_T \rho_T \frac{\partial T}{\partial \tau} dx = \int_0^l \lambda_T \frac{\partial^2 T}{\partial x^2} dx \quad (2)$$

The coefficients  $c_T$ ,  $\rho_T$  and  $\lambda_T$  change insignificantly as the temperature of the plate increases before melting begins, so we accept them as constant values independent of temperature. Taking into account the above, Eq. (2) becomes:

**Figure 6** Scheme of the process of heating a solid body in the form of a thin metal plate with a flow of superheated melt.



$$c_T \rho_T \int_0^l \frac{\partial T}{\partial \tau} dx = \lambda_T \int_0^l \frac{\partial}{\partial x} \frac{\partial T}{\partial x} dx \tag{3}$$

Considering that, according to Fourier’s law of thermal conductivity  $q = -\lambda \frac{\partial T}{\partial x}$ , we have

$$-c_T \rho_T \int_0^l \frac{\partial T}{\partial \tau} dx = \int_0^l \frac{\partial q}{\partial x} dx = \int_0^l dq \tag{4}$$

Thus,

$$-c_T \rho_T \int_0^l \frac{\partial T}{\partial \tau} dx = q(l, \tau) - q(0, \tau) \tag{5}$$

Taking into account the small thickness of the plate (in comparison with the size of the melt flow), it is advisable to assume equality of plate temperatures at its boundaries at  $x = 0$  and  $x = l$ , i.e.

$$T(0, \tau) \approx T(l, \tau) \tag{6}$$

Now Eq. (5) looks like

$$-c_T \rho_T \frac{\partial T}{\partial \tau} l = q(l, \tau) - q(0, \tau) \tag{7}$$

The heat flux density  $q(0, \tau)$  is determined by the law of convective heat transfer

$$q(0, \tau) = \alpha(T_{av.m} - T) \tag{8}$$

where  $T_{av.m} = \text{const}$ —average melt temperature in the melting chamber; as a first approximation  $T_{av.m}$ , it can be taken as the arithmetic mean of the melt temperatures at the inlet and outlet of the melting unheated chamber, K;  $T = T(\tau)$ —current value of the plate temperature, K.

The heat flux density  $q(l, \tau)$  can be determined based on the laws of convective heat transfer or thermal radiation.  $q(l, \tau)$  can also be expressed by the law of total heat transfer. Herewith, taking into account the obvious short duration of the process of heating the plate to the melting temperature, we will neglect the value  $q(l, \tau)$ . In this case, it is assumed that the plate accumulates all the heat supplied from the melt flow. In this case, Eq. (7) becomes

$$c_T \rho_T \frac{\partial T}{\partial \tau} = \alpha(T_{av.m} - T) \tag{9}$$

Equation (9) can be solved, for example, by numerical methods, but for this it is necessary to know the value of the heat transfer coefficient  $\alpha$ . The result of such solution will be the dependence of its heating before the melting start.

The melting process of the plate was considered (see Fig. 6). We assume that the plate temperature is maintained constant throughout the entire process and equal to the melting temperature  $T_{mel}$  of the alloy. In this case, the heat supplied to the surface of the plate is consumed for its melting.

The differential equation for the plate melting process looks like [61, 62]:

$$\alpha(T_{av.m} - T_{mel})F d\tau = L dm \tag{10}$$

where  $L$ —specific aluminium alloy melting heat, J/kg;  $m$ —plate mass, kg.

According to Eq. (10), elementary mass  $dm$  is melted during elementary time  $d\tau$ .

The plate melting speed is determined from the following expression

$$\frac{dm}{d\tau} = \frac{\alpha(T_{av.m} - T_{mel})F}{L} \tag{11}$$

To estimate the plate melting time, Eq. (11) has been integrated over time from the moment  $\tau_1$ , i.e. melting start, to  $\tau_2$ —melting end:

$$\int_{\tau_1}^{\tau_2} \frac{dm}{d\tau} d\tau = \int_{\tau_1}^{\tau_2} \frac{\alpha(T_{av.m} - T_{mel})F}{L} d\tau \tag{12}$$

and

$$m(\tau_2) - m(\tau_1) = \frac{\alpha(T_{av.m} - T_{mel})F}{L} (\tau_2 - \tau_1) \tag{13}$$

where  $m(\tau_1)$ —mass of molten metal at a moment in time  $\tau_1$ , kg;  $m(\tau_2)$ —molten metal mass at a moment in time  $\tau_2$ , kg.

Since  $m(\tau_1) = 0$ , and  $m(\tau_2) = m$ , then the melting time  $\tau_m$  of entire plate will be

$$\tau_m = \tau_2 - \tau_1 = \frac{m \cdot L}{\alpha(T_{av.m} - T_{mel})F} \tag{14}$$

So, the most important equations of the process under study are (9), (11) and (14). But these equations cannot be solved, since the convection heat transfer coefficient is unknown. In addition, the actual process involves heating and melting of the charge layer.

Unlike a plate, in such a layer the temperature is distributed non-uniformly, which complicates the formulation of the problem and its solution.

In this regard, an experiment is needed that would allow us to determine the coefficient taking into account the features of the real process.

In order to specify the conditions for conducting such an experiment and identify all the required parameters on the experimental equipment, we will study the process of melting a portion of an aluminium charge with a mass of  $M_{por}$ , placed on the surface  $S_K$  of the melt in an unheated melting chamber (Fig. 7). In the case when the height of the charge layer along the length of the chamber is the same, its current value is equal to  $h^*$ .

The thermal process from the initial moment of time ( $\tau = 0$ ) of the “instantaneous” filling of the charge on the melt surface was analysed. The entire charge was assumed to be stationary and in contact with the melt only in the plane of its surface  $S_K$ , i.e. the possibility of immersion of individual charge bodies into the melt was excluded.

The bodies (particles) of the finely dispersed thin-walled charge, in direct contact with the melt, are heated to the melting temperature at a very high speed. Therefore, when studying the process of melting a charge in a melt flow, it is advisable to exclude the short-term stage of heating a relatively thin layer of bodies in contact with the melt flow at the initial moment of time.

Thus, instantaneous heating of the charge across the contact surface  $S_K$  to the melting point was assumed. During the entire process of melting a portion of the

charge, the temperature on such a surface is maintained constant  $T_{mel}$ . It was assumed that the melt flow rate at the outlet of the melting chamber would be greater than at the inlet by the value of the charge melting rate. In this case, the melt level in the melting chamber will be stable. It is clear that when the metal is melted from the boundary surface  $S_K$ , the charge bodies located above  $S_K$  are simultaneously heated, which gradually descend to the surface of the melt flow, heating up to a temperature  $T_{mel}$ .

The differential equation of the melting process of the charge portion was represented as

$$\alpha(T_{av.m} - T_{mel})S_K d\tau = -\lambda_{ef} \frac{\partial T}{\partial x} S_K d\tau + LdM_{por} \quad (15)$$

where  $\lambda_{ef}$ —effective coefficient of thermal conductivity of the charge material, taking into account the dispersion of the latter in the bulk state,  $W/(m \cdot K)$ .

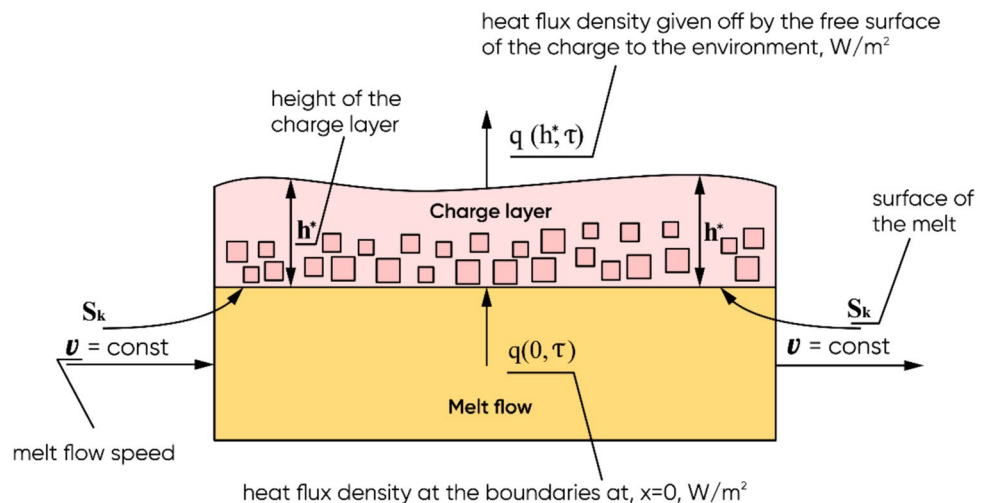
Equation (15) can be rewritten as follows

$$\alpha(T_{av.m} - T_{mel})S_K = -\lambda_{ef} \frac{\partial T}{\partial x} S_K + L \frac{dM_{por}}{d\tau} \quad (16)$$

where  $\frac{dM_{por}}{d\tau}$ —melting speed, kg/s.

Equations (15) and (16) are heat balances. The left side in (15) represents the amount of heat supplied from the melt flow to the surface  $S_K$  of the charge portion during elementary time  $d\tau$ . This heat is consumed partly on melting the elementary mass of the alloy  $dM_{por}$  (the second summand on the right side in (15)) and partly on heating the part of the charge that has not been melted at a given time (the first summand on the right side in (15)). Obviously, the right side in Eqs. (15) and (16) is represented by a sum, since  $\frac{\partial T}{\partial x} < 0$

**Figure 7** Scheme of the process of heating and melting a thin-walled aluminium charge with a developed surface in a flow-through unheated melting chamber of an experimental MHD circulation circuit with MDP.



The heat flux from the melting boundary into the charge layer was expressed from Eq. (16):

$$-\lambda_{ef} \frac{\partial T}{\partial x} S_K = \alpha (T_{av.m} - T_{mel}) S_K - L \frac{dM_{por}}{d\tau} \quad (17)$$

where  $\alpha (T_{av.m} - T_{mel}) S_K = \text{const}$

After multiplying Eq. (5) by  $S_K$ , the following was obtained:

$$c_T \rho_T S_K \int_0^l \frac{\partial T}{\partial \tau} dx = q(0, \tau) S_K - q(l, \tau) S_K \quad (18)$$

Equation (18) is written for a plate. It has been rewritten for the charge layer. Considering that  $q(0, \tau) S_K = -\lambda_{ef} \frac{\partial T}{\partial x} S_K$ , we will get from Eqs. (17) and (18):

$$c_{ef} \rho_{ef} S_K \int_0^{h^*} \frac{\partial T}{\partial \tau} dx = \left( \alpha (T_{av.m} - T_{mel}) S_K - L \frac{dM_{por}}{d\tau} \right) - q(h^*, \tau) S_K \quad (19)$$

where  $c_{ef}$ —effective value of the heat capacity of the charge material, J/(kg·K);  $\rho_{ef}$ —effective density of the charge material, kg/m<sup>3</sup>;  $q(h^*, \tau)$ —density of heat flux given off by the free surface of the charge to the environment, W/m<sup>2</sup>.

As is known, at a body surface temperature below 500 K (227 °C), the main heat transfer to the air is carried out by convection; at higher temperatures, above 1000 K (727 °C)—by thermal radiation. Since the temperature of the free surface of the aluminium charge layer in the unit chamber changes during the melting process from 20 °C (or any other temperature) to melting temperature for aluminium  $T_{mel}$  (660 °C), we will express the surface flux density as follows:

$$q(h^*, \tau) = \alpha_K (T(h^*, \tau) - T_C) + k \cdot \varepsilon \cdot T(h^*, \tau)^4 \quad (20)$$

where  $\alpha_K$ —heat transfer coefficient by convection from the boundary surface at  $h^*$ , (W/(m<sup>2</sup>·K));  $T(h^*, \tau)$ —boundary surface temperature, K;  $T_C = 293.15$  K (20 °C)—ambient temperature;  $k$ —Stefan-Boltzmann constant,  $5.67 \cdot 10^{-8}$  W/(m<sup>2</sup>·K<sup>4</sup>);  $\varepsilon$ —body surface emissivity coefficient; for aluminium polished at temperatures from 500 to 800 K  $\varepsilon = 0.039 - 0.057$  [61–64].

The coefficient  $\alpha_K$  estimation was performed. With natural air convection, the Nusselt number is [61, 62, 65]

$$Nu = C(\text{Pr} \cdot \text{Gr})^n \quad (21)$$

where  $C$  and  $n$ —coefficients;  $\text{Pr}$ —Prandtl number;  $\text{Gr}$ —Grashof number, determined by the formula [61, 62, 65]:

$$\text{Gr} = \beta \frac{g \cdot l_T^3}{\nu^2} \Delta T \quad (22)$$

where  $\beta$ —volume-expansion coefficient, 1/°C;  $g$ —gravity acceleration, m/s<sup>2</sup>;  $l_T$ —characteristic size of the streamlined body (for a horizontally located layer of charge in the chamber—the smallest size (m); in this case ~ 0.1 m);  $\nu$ —kinematic viscosity, m<sup>2</sup>/s;  $\Delta T$ —temperature difference at the boundary of a streamlined body, °C.

The physical constants for air, which are part of the similarity numbers, are determined by the average temperature of the boundary layer in °C. The average temperature of the free surface of the charge layer in the chamber during the melting process is equal to

$$T_{S.av} = \frac{20 + 660}{2} = 340^\circ\text{C} \quad (23)$$

Then, the average temperature of the boundary layer of air will be:

$$T_b = \frac{T_{S.av} + T_C}{2} = \frac{340 + 20}{2} = 180^\circ\text{C} \quad (24)$$

For dry air at normal atmospheric pressure (0.1 MPa), a temperature of 180 °C corresponds to [66, 67]:

- (1) kinematic viscosity  $\nu = 32.49 \cdot 10^{-6}$  m<sup>2</sup>/s;
- (2) volume-expansion coefficient  $\beta = 22.1 \cdot 10^{-6}$  1/°C;
- (3) Prandtl number  $\text{Pr} = 0.681$ ;
- (4) coefficient of thermal conductivity  $\lambda_B = 3.78 \cdot 10^{-2}$  W/(m·K).
- (5) In this case, we define  $\Delta T$  as the difference between the average temperature of the surface of the charge layer  $T_{S.av}$  during the melting process and the ambient air temperature

$$\Delta T = 340 - 20 = 320^\circ\text{C} \tag{25}$$

Thus, we will get

$$\text{Gr} = \frac{9.81 \cdot 0.1^3}{(32.49 \cdot 10^{-6})^2} \cdot 22.1 \cdot 10^{-4} \cdot 320 = 65.7 \cdot 10^5 \tag{26}$$

The product  $\text{Pr} \cdot \text{Gr}$  will be:

$$\text{Pr} \cdot \text{Gr} = 0.681 \cdot 65.7 \cdot 10^5 = 44.74 \cdot 10^5 \tag{27}$$

According to the data [66, 67], in case  $5 \cdot 10^2 < \text{Pr} \cdot \text{Gr} < 2 \cdot 10^7$  the coefficients will be:  $C = 0.7$  and  $n = 0.25$ .

Substituting all the necessary values into Eq. (21), we will obtain

$$\text{Nu} = 0.7(0.681 \cdot 65.7 \cdot 10^5)^{0.25} = 32.18 \tag{28}$$

Considering that, according to [61, 62, 65], the Nusselt criterion can be expressed as

$$\text{Nu} = \frac{\alpha_K \cdot l_T}{\lambda_B} \tag{29}$$

we have:

$$\alpha_K = \frac{\text{Nu} \cdot \lambda_B}{l_T} = \frac{32.18 \cdot 3.78 \cdot 10^{-2}}{0.1} = 12.16 \text{ W}/(\text{m}^2 \cdot \text{K}) \tag{30}$$

So, the approximate value of the coefficient  $\alpha_K$  is determined. Returning to expressions (19) and (20), substitute (20) into Eq. (13) and then obtain:

$$c_{\text{ef}} \rho_{\text{ef}} S_K \int_0^{h^*} \frac{\partial T}{\partial \tau} dx = \left[ \alpha(T_{\text{av.m}} - T_{\text{mel}}) \cdot S_K - L \frac{dM_{\text{por}}}{d\tau} \right] - [\alpha_K(T(h^*, \tau) - T_C) \cdot S_K + 5.67 \cdot 10^{-8} \cdot \varepsilon \cdot T(h^*, \tau)^4 \cdot S_K] \tag{31}$$

When considering the actual temperature distribution at the segment  $(0, h^*)$ , we proceeded to its average integral value  $T_{\text{av}}$ . This temperature is a function of time only, and the derivative  $\frac{\partial T}{\partial \tau}$  characterizing the change in time of the average integral temperature of the charge layer can be taken out of the sign of the integral. As a result, Eq. (31) will take the form:

$$c_{\text{ef}} \rho_{\text{ef}} S_K \frac{\partial T_{\text{av}}}{\partial \tau} \cdot h^* = \left[ \alpha(T_{\text{av.m}} - T_{\text{mel}}) \cdot S_K - L \frac{dM_{\text{por}}}{d\tau} \right] - [\alpha_K(T(h^*, \tau) - T_C) \cdot S_K + 5.67 \cdot 10^{-8} \cdot \varepsilon \cdot T(h^*, \tau)^4 \cdot S_K] \tag{32}$$

From the product  $\rho_{\text{ef}} \cdot S_K \cdot h^*$  we obtain the current value of the charge mass  $M_{\text{ch}}(\tau)$  as a function of time. We rewrite Eq. (32) as:

$$c_{\text{ef}} M_{\text{ch}}(\tau) \frac{\partial T_{\text{av}}}{\partial \tau} = \left[ \alpha(T_{\text{av.m}} - T_{\text{mel}}) \cdot S_K - L \frac{dM_{\text{por}}}{d\tau} \right] - [\alpha_K(T(h^*, \tau) - T_C) \cdot S_K + 5.67 \cdot 10^{-8} \cdot \varepsilon \cdot T(h^*, \tau)^4 \cdot S_K] \tag{33}$$

The resulting differential equation characterizes the change in the heat content of the charge mass  $M_{\text{ch}}(\tau)$  during the melting process.

Equation (33) was extended to the whole charge melting process. The following was obtained as a result:

$$c_{\text{ef}} \int_0^{\tau_m} M_{\text{ch}}(\tau) \frac{\partial T_{\text{av}}}{\partial \tau} d\tau = \int_0^{\tau_m} \alpha(T_{\text{av.m}} - T_{\text{mel}}) \cdot S_K d\tau - \int_0^{\tau_m} \frac{dM_{\text{por}}}{d\tau} d\tau - \int_0^{\tau_m} \alpha_K(T(h^*, \tau) - T_C) \cdot S_K d\tau - 5.67 \cdot 10^{-8} \int_0^{\tau_m} \varepsilon T(h^*, \tau)^4 \cdot S_K d\tau \tag{34}$$

or

$$C_{\text{ef}} \int_{T_{\text{in}}}^T M_{\text{ch}}(T_{\text{av}}) dT_{\text{av}} = \int_0^{\tau_m} \alpha(T_{\text{av.m}} - T_{\text{mel}}) \cdot S_K d\tau - \int_0^{M_{\text{por}}} L dM_{\text{por}} - \int_0^{\tau_m} \alpha_K(T(h^*, \tau) - T_C) \cdot S_K d\tau - 5.67 \cdot 10^{-8} \int_0^{\tau_m} \varepsilon T(h^*, \tau)^4 \cdot S_K d\tau \tag{35}$$

where  $M_{\text{ch}}(T_{\text{av}})$ —current value of the charge mass as a function of the average integral temperature, kg;  $T_{\text{in}}$ —initial charge temperature, K;  $dT_{\text{av}}$ —full differential of average integral temperature, K.

Taking  $\alpha$ ,  $L$ ,  $\alpha_K$ ,  $\varepsilon$  as constant values, as well as considering that  $S_K = \text{const}$ , was received:

$$c_{ef} \int_{T_{in}}^{T_{mel}} M_{ch}(T_{av}) dT_{av} = \alpha(T_{av,m} - T_{mel}) \cdot S_K \tau_m - L \cdot M_{por} - \alpha_K S_K \int_0^{\tau_m} (T(h^*, \tau) - T_C) d\tau - 5.67 \cdot 10^{-8} \cdot \epsilon \cdot S_K \int_0^{\tau_m} T(h^*, \tau)^4 d\tau \quad (36)$$

To simplify, we replace the temperature function of the free surface  $T(h^*, \tau)$  of the charge layer with its arithmetic mean value. As a result, Eq. (29) will take the form:

$$c_{ef} \int_{T_{in}}^{T_{mel}} M_{ch}(T_{av}) dT_{av} = \alpha(T_{av,m} - T_{mel}) \cdot S_K \cdot \tau_m - L \cdot M_{por} - \alpha_K \cdot S_K (T_{S,av} - T_{av}) \cdot \tau_m - 5.67 \cdot 10^{-8} \cdot \epsilon \cdot S_K T_{S,av}^4 \cdot \tau_m \quad (37)$$

In Eq. (37), the function  $M_{ch}(T_{av})$  is unknown and must be specified correctly. For this purpose, the previously mentioned Eq. (33) was analysed. On the left side of Eq. (33) we have a change in the thermal power of the charge layer. Over time, the temperature of such a layer increases and is distributed more and more uniformly, and the difference  $(T_{mel} - T_{av})$  decreases. This helps to reduce the heating rate  $\frac{\partial T_{av}}{\partial \tau}$  of the layer. The current mass value  $M_{ch}(\tau)$  gradually decreases to zero.

Thus, the rate of change in the thermal power of the charge layer in the process of continuous accumulation of heat and melting (the left side in Eq. (33)) decreases. The free surface of the layer was assumed to be thermally insulated, i.e. heat fluxes by convection and radiation are equal to zero in Eq. (33). Then, taking into account that a time-constant heat flux  $\alpha(T_{av,m} - T_{mel}) \cdot S_K = \text{const}$  is supplied to the melting surface, a decrease in the change in the thermal power of the charge layer is realized by increasing the amount of heat  $L \frac{dM_{por}}{d\tau}$  spent directly on melting. Here-with, the melting rate  $\frac{dM_{por}}{d\tau}$  increases, which reaches its maximum value towards the end of the process.

On the contrary, the heat flux  $\alpha(T_{av,m} - T_{mel}) \cdot S_K - L \frac{dM_{por}}{d\tau}$  passing through the melting front decreases with time.

In this case, the charge layer is modelled as a porous body that is heated through. Therefore, heat fluxes by convection and radiation removed from the free surface of the layer (the terms in the second square brackets of Eq. (33)) make an additional

contribution to reducing the change in the thermal power of the layer.

Taking into account the above, and also, since at  $\tau = 0$  the average integral layer temperature is  $T_{av} = T_{in}$  and at  $\tau = \tau_m - T_{av} = T_{mel}$ , it is advisable to represent the function of changing the mass of the layer  $M_{ch}(T_{av})$  approximately in the form of a second-order parabola (Fig. 8):

$$M_{ch}(T_{av}) = M_{por} - M_{por} \left( \frac{T_{av} - T_{in}}{T_{mel} - T_{in}} \right)^2 \quad (38)$$

Expression (38) has been verified. At  $T_{av} = T_{in}$  was obtained:

$$M_{ch}(T_{in}) = M_{por} - M_{por} \left( \frac{T_{in} - T_{in}}{T_{mel} - T_{in}} \right)^2 = M_{por} \quad (39)$$

If  $T_{av} = T_{mel}$ , then

$$M_{ch}(T_{mel}) = M_{por} - M_{por} \left( \frac{T_{mel} - T_{in}}{T_{mel} - T_{in}} \right)^2 = 0 \quad (40)$$

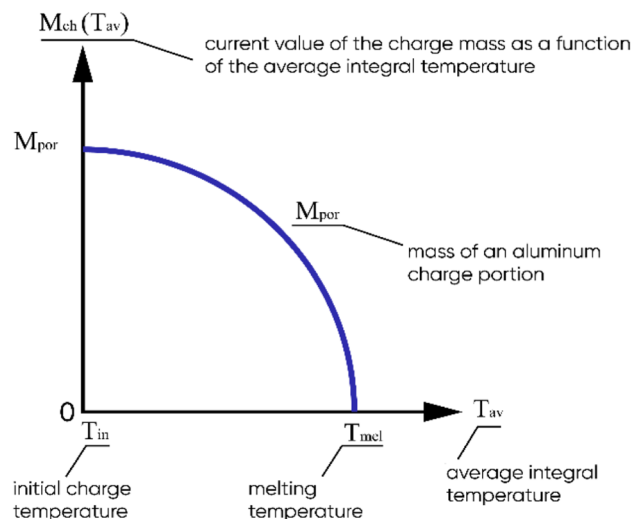


**Figure 8** Dependence of the mass of solid charge that can be melted in a flow of superheated melt on its average integral temperature.

This expression has been integrated over a range of temperatures  $T_{in} < T_{av} < T_{mel}$ :

$$\begin{aligned} & \int_{T_{in}}^{T_{mel}} \left[ M_{por} - M_{por} \left( \frac{T_{av} - T_{in}}{T_{mel} - T_{in}} \right)^2 \right] \cdot dT_{av} \\ &= \int_{T_{in}}^{T_{mel}} M_{por} dT_{av} - \frac{M_{por}}{(T_{mel} - T_{in})^2} \times \int_{T_{in}}^{T_{mel}} (T_{av} - T_{in})^2 dT_{av} \\ &= M_{por} \cdot T_{av} \Big|_{T_{in}}^{T_{mel}} - \frac{M_{por}}{(T_{mel} - T_{in})^2} \cdot \frac{(T_{av} - T_{in})^3}{3} \Big|_{T_{in}}^{T_{mel}} \quad (41) \\ &= M_{por} (T_{mel} - T_{in}) - \frac{1}{3} \frac{M_{por}}{(T_{mel} - T_{in})^2} (T_{mel} - T_{in})^3 \\ &= \frac{2}{3} M_{por} (T_{mel} - T_{in}) \end{aligned}$$

Substituting the resulting value of the integral into the left side of expression (37), and received:

$$\begin{aligned} & \frac{2}{3} \cdot c_{ef} \cdot M_{por} (T_{mel} - T_{in}) = \alpha (T_{av.m} - T_{mel}) \\ & \cdot S_K \tau_m - LM_{por} - \alpha_K S_K (T_{S.av} - T_C) \quad (42) \\ & \cdot \tau_m - 5.67 \cdot 10^{-8} \cdot \epsilon \cdot S_K T_{S.av}^4 \tau_m \end{aligned}$$

Equation (42) was solved with respect to  $\alpha \cdot S_K$ :

$$\begin{aligned} \alpha \cdot S_K &= 0.667 \frac{c_{ef} M_{por}}{\tau_m} \cdot \frac{T_{mel} - T_{in}}{T_{av.m} - T_{mel}} \\ &+ \frac{L \cdot M_{por}}{\tau_m (T_{av.m} - T_{mel})} + \alpha_K \cdot S_K \frac{T_{S.av} - T_{av}}{T_{av.m} - T_{mel}} \\ &+ 5.67 \cdot 10^{-8} \cdot \epsilon \cdot S_K \frac{T_{S.av}^4}{T_{av.m} - T_{mel}} \quad (43) \end{aligned}$$

When setting the problem, it has been assumed that heat is supplied to a portion of the charge through the boundary surface  $S_K$  of the melt, which is flat. In this case, the free surface of the charge layer was also considered as flat and was equal to  $S_K$ . However, the actual process of melting the charge is more complicated. In this case, the layer in the chamber consists of a large number of small bodies and its actual surface  $S_{Sb}$ , through which heat is transferred from the melt, is curved. Obviously  $S_K > S_s$ . The size of the free surface of the real layer, due to the homogeneous distribution of the density of the charge in the bulk state, can be taken statistically equal to  $S_{Sb}$ . Taking into account the above, the real surfaces of the charge layer were considered, replacing in formula (36)  $S_K$  by  $S_{Sb}$ . In

addition, it is advisable here to express the mass of a portion through  $S_{Sb}$ :

$$M_{por} = \rho_{ef} \cdot H_{in} \cdot S_{Sb} \quad (44)$$

where  $H_{in}$ —height (thickness) of the initial charge layer in the chamber, m.

Formula (43) will be presented in the form:

$$\begin{aligned} \alpha \cdot S_{Sb} &= 0.667 \frac{c_{ef} \rho_{ef} H_{in} S_{Sb}}{\tau_m} \cdot \frac{T_{mel} - T_{in}}{T_{av.m} - T_{mel}} \\ &+ \frac{L \rho_{ef} H_{in} S_{Sb}}{\tau_m (T_{av.m} - T_{mel})} + \alpha_K S_{Sb} \frac{T_{S.av} - T_C}{T_{av.m} - T_{mel}} \quad (45) \\ &+ 5.67 \cdot 10^{-8} \cdot \epsilon \cdot S_{Sb} \frac{T_{S.av}^4}{T_{av.m} - T_{mel}} \end{aligned}$$

By dividing formula (45) by  $S_{Sb}$ , we will finally get

$$\begin{aligned} \alpha &= 0.667 \frac{c_{ef} \rho_{ef} H_{in}}{\tau_m} \cdot \frac{T_{mel} - T_{in}}{T_{av.m} - T_{mel}} \\ &+ \frac{L \rho_{ef} H_{in}}{\tau_m (T_{av.m} - T_{mel})} + \alpha_K \frac{T_{S.av} - T_C}{T_{av.m} - T_{mel}} \quad (46) \\ &+ 5.67 \cdot 10^{-8} \cdot \epsilon \cdot \frac{T_{S.av}^4}{T_{av.m} - T_{mel}} \end{aligned}$$

From formula (46) an obvious conclusion follows: to calculate the value of the coefficient, it is necessary to experimentally determine the time of complete melting  $\tau_m$  of an arbitrary portion of the charge at certain fixed values of the melt temperature and flow rate.

The study of the melting process of a charge with a developed surface in the melting chamber of the MHD circuit should be carried out according to formulas (11) and (14). Assuming that  $F = S_K \approx S_{Sb}$ , as well as substituting plate mass ( $m$ ) be portion mass ( $M_{por}$ ), was received:

$$\frac{dM_{por}}{d\tau} \approx \frac{\alpha (T_{av.m} - T_{mel}) \cdot S_K}{L} \quad (47)$$

and

$$\tau_m \approx \frac{M_{por} \cdot L}{\alpha (T_{av.m} - T_{mel}) \cdot S_K} \quad (48)$$

Using formula (47), the approximate value of the maximum (close to the maximum) melting rate of the charge corresponding to the specific mode (values  $T_{av.m} = \text{const}$  and  $v = \text{const}$ ) of melting is calculated.

The average melting rate ( $v_{\text{mel.av}}$ ) of the entire portion of the charge, weighing  $M_{\text{por}}$ , can be calculated using the following approximate formula

$$V_{\text{mel.av}} \approx \frac{1}{2} \frac{\alpha (T_{\text{av.m}} - T_{\text{mel}}) \cdot S_K}{L} \quad (49)$$

Now that a method for analytical evaluation of the process under investigation has been developed, possible aspects of technology optimization should be considered. Firstly, when switching from an experimental to an industrial design, it may be necessary to ensure the specified performance of the unit. To solve this problem, one should use formula (49). Indeed, the rate of melting of the charge in this case is the productivity of the device. It can be ensured by the appropriate area  $S_K$  of the melting chamber area. Having designated the hourly productivity as  $\pi$  (t/hour), the required area of the melting chamber can be calculated using the formula:

$$S_K = \frac{2}{3.6} \frac{\pi \cdot L}{\alpha (T_{\text{av.m}} - T_{\text{mel}})} = 0.556 \frac{\pi \cdot L}{\alpha (T_{\text{av.m}} - T_{\text{mel}})} \quad (50)$$

where 3.6—coefficient, s/kg.

Secondly, it is possible to optimize the electrical parameters of the inductor and electromagnet of the MDP. It is clear that with a simultaneous increase in the temperature of the melt and the rate of metal flow in an unheated melting chamber, the rate of melting of the charge should also increase, and therefore the productivity of the installation, but this can lead to a disproportionate increase in energy costs.

An interesting experiment in this regard is to determine the melting rate of the charge at various combinations of melt temperature and flow rate. It is quite possible that with the combination of “maximum flow rate (upper factor level) at the minimum possible melt temperature (lower factor level)” or, conversely, “maximum possible melt temperature at minimum flow rate”, the savings in electrical energy will be more significant than reduction in plant productivity. Therefore, an optimal solution is possible.

There are the available data various researchers and companies [2, 45–50]. For saving energy resources with synchronous high productivity of the remelting process, it is considered more preferable to implement a mode with the maximum possible (determined by the pump power) melt circulation rate at the same time the relatively low temperature of its overheating above the liquidus temperature. That is, the dominant

factor in this method of remelting is convective heat and mass transfer in the system “overheated moving melt—solid charge” and related effects and phenomena.

The design features of the MDP should also be taken into account. If in circuits with an electromagnetic pump of travelling field, the pump only provides circulation of the melt in the melting circuit. At application of the MDP, thanks to the presence of two independent electromagnetic systems—an inductor and an electromagnet—it is possible to simultaneously control both the temperature of the melt and the speed of its movement within a wide range.

Thus, MDP provides much greater and more substantial opportunities & benefits for controlling the thermal and hydrodynamic parameters of the process of remelting aluminium scrap and waste.

Finally, if we consider all these aspects in a complex, then as a result of the experiment a polynomial relationship can be obtained

$$\alpha = f(T_{\text{av.m}}, V) \quad (51)$$

It can be used in formulas (47), (48), (59) and (50). Obviously, by changing the convective heat transfer coefficient  $\alpha$ , it is possible to vary the melting modes and calculate the process characteristics for each of them, similar to how it's done in other high-energy methods [16, 17, 68, 69].

### MHD circulation circuit and its thermal calculation

In the process under study, the following technological parameters are decisive: (1) temperature  $t_1$  (°C) and mass feed rate  $Q_1$  (using the MDP) into an unheated chamber of liquid aluminium alloy from a crucible attached to the MDP; (2) temperature  $t_2$  (°C) and mass velocity  $Q_2$  of the liquid metal removed from the unheated chamber after melting the aluminium charge; (3) temperature  $t_3$  (°C) and mass flow rate  $Q_3$  of solid aluminium charge into the unheated chamber.

Before conducting direct field studies, a preliminary calculation of the parameters of the described process was performed. In this case, the assessment of the heat content (thermal power) introduced into the unheated chamber by the original liquid aluminium alloy was made according to the equation [70]:



$$j_1 = Q_1 \cdot t_1 \cdot C_1, W \tag{52}$$

where  $C_1$ —heat capacity of the melt entering the unheated melting chamber at  $t_1$ , J/kg·°C.

It was also accepted that the thermal power  $j_1$  introduced by the melt into the unheated chamber is consumed as follows:

$$j_1 = P + j_2 + \Delta j_3, W \tag{53}$$

where  $P$ —heat loss in an unheated chamber, W;  $j_2$ —power carried away from an unheated chamber by the melt flow into a heated chamber, W;  $\Delta j_3$ —power spent on melting the charge, W.

Thermal losses of an unheated chamber in general should be calculated as the sum of losses through the walls of the chamber and losses from the surface of the melt. However, in our case, the following preliminary experiment was carried out without supply the charge and melting it in an unheated chamber. The temperature drop during the circulation of the liquid metal along the contour between the heated and unheated chambers was simply estimated. The temperature of the melt at the exit from the MDP and the entrance to the unheated melting chamber at the initial moment after starting the circuit was 790 °C. After a complete cycle of melt circulation through the circuit the loss of its temperature did not exceed 3–4 °C. It slightly exceeds the temperature measurement error. Therefore, at the first stage of research, this heat loss was not taken into account in further calculations.

The heat content (thermal power) of the melt removed from the unheated chamber back to the heated chamber was determined using a formula similar to (52):

$$j_2 = Q_2 \cdot t_2 \cdot C_2 \tag{54}$$

where  $C_2$ —heat capacity of the melt flowing from an unheated chamber, J/kg·°C.

To ensure the stability of the process in general, the following condition must be met:

$$Q_2 = Q_1 + Q_3, \text{ Kg/s} \tag{55}$$

In fact, as the charge melts, in accordance with the principle of communicating vessels, there is an increase in the level of the melt in the entire system.

Change in the heat content of the initially solid charge (the power spent on its melting):

$$\Delta j_3 = Q_3 \cdot (t_2 \cdot C_2 - t_3 \cdot C_3), W \tag{56}$$

where  $C_3$ —heat capacity of a solid charge at the temperature of its feed to an unheated chamber  $t_3$ , J/kg·°C.

Taking into account the above considerations and expressions (52)–(56), we can write an equation that in general relates the relationship between thermal and flow parameters:

$$Q_1 \cdot t_1 \cdot C_1 = (Q_1 + Q_3) \cdot t_2 \cdot C_2 + Q_3 \cdot (t_2 \cdot C_2 - t_3 \cdot C_3) \tag{57}$$

By solving Eq. (57), in our case it was necessary to determine the rate of mass supply of solid charge  $Q_3$  to the liquid metal surface in an unheated chamber of an experimental MHD circulation melting circuit:

$$Q_3 = \frac{Q_1 \cdot (t_1 \cdot C_1 - t_2 \cdot C_2)}{2 \cdot t_2 \cdot C_2 - t_3 \cdot C_3} \text{ Kg/s} \tag{58}$$

Before the start of a complex full-scale experiment, a calculation was made of the process of remelting the charge, which is a container (cans) for drinks and, in terms of its chemical composition, consists of almost pure aluminium.

Initial data for calculation for pure aluminium:

$$Q_1 = 1.2 \text{ kg/s}; t_1 = 750 \text{ °C}; C_1 = 1.02 \cdot 10^3 \text{ J/kg} \cdot \text{°C}; t_2 = 680 \text{ °C}; C_2 = 1 \cdot 10^3 \text{ J/kg} \cdot \text{°C}; t_3 = 100 \text{ °C}; C_3 = 0.942 \cdot 10^3 \text{ J/kg} \cdot \text{°C};$$

$$\text{Then } Q_3 = 0.065 \text{ Kg/s.}$$

Turning to the mass of the metal, we find that 1 kg of solid charge melts in the unheated chamber in about 15 s. For pure aluminium, the ratio of the rate of supply of the melt and solid charge into the melting chamber at the initial temperature of the liquid metal of 750 °C and a final temperature of the withdrawn melt of 680 °C should be within the limits

$$k = \frac{Q_1}{Q_3} \approx 18.5 \tag{59}$$

i.e. for the specified temperature conditions, the mass rate of supply of the initial melt into the unheated melting chamber should be approximately 18–19 times higher than the rate of supply of the solid charge for melting.

## Discussion

### Experimentation and analysis of results

After the prototype of the circulation melting circuit was put into operation, a portion of the charge was

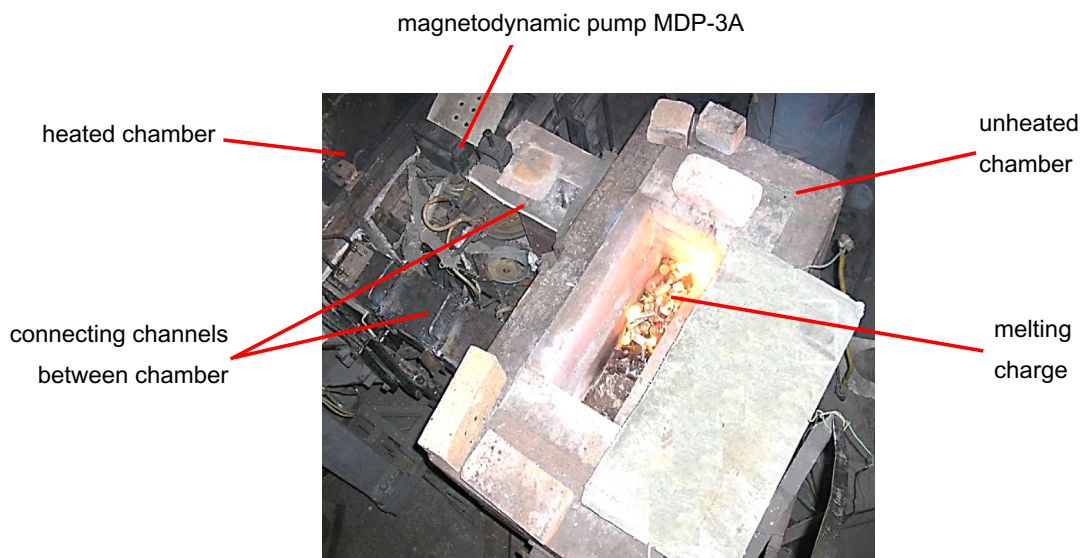
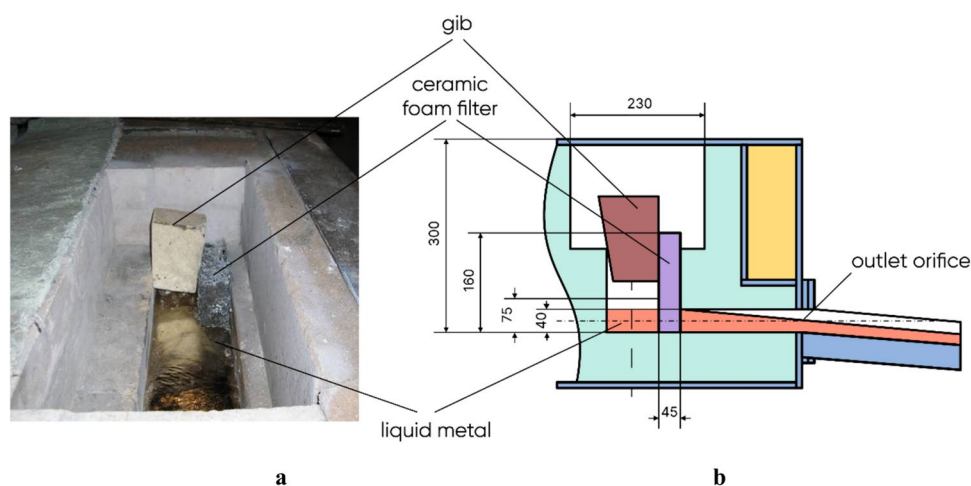


**Figure 9** Melting of a thin-walled aluminium charge on the surface of the melt in the unheated chamber of the experimental circuit.

**Figure 10** Ceramic foam filter installed at the outlet of the unheated melting chamber of the experimental circuit: **a** filter in the circuit; **b** filter installation diagram.



supplied onto the surface of the liquid aluminium flow in the unheated melting chamber (Fig. 9).

The following feature was established during the experiment. There is oxide ( $\text{Al}_2\text{O}_3$ ) film on the surface of the liquid metal bath. When the thickness of the charged fine scrap layer is up to 200 mm, due to its low average bulk density, it is not immediately immersed into the melt and is not carried away by the flow. This scrap portion lies on the surface of the liquid metal bath for some time held by a oxide film, and it gradually melts relatively slowly from below by overheated moving melt. In this case, the paint and varnish coatings on the surface of the charge burn out, organic contaminants and moisture are removed. The charge itself

is slightly oxidized, and gaseous combustion products do not enter the liquid metal.

As the charge melted, slag, consisting of solid products of burnt coatings and aluminium oxide, accumulated on the flow surface. The slag was periodically removed and remelting continued as before. To more completely prevent the entry of oxide and other solid inclusions into the melt, a ceramic foam filter was installed at the outlet of the unheated melting chamber (Fig. 10).

In the initial modes of remelting, there was relatively low level of melt in the system. In order to avoid clogging of the working (filtering) surface of the filter with slag and dross, with the help of MDP excess pressure was created. The value of this pressure makes

**Table 2** Changing chemical composition of experimental alloy for during remelting process

Alloy	Content of the main elements, % by weight					
	Al	Si	Fe	Mg	Ti	Cu
Initial (at start of circuit with 80 kg of melt)	Basic	0.25	0.20	0.30	0.10	0.10
Final (after remelting the waste portion of 20 kg)	Basic	0.28	0.26	0.29	0.10	0.11

such height of the rise of the metal in the unheated melting chamber that was higher than the level of the upper cut of the ceramic foam filter. In this case, it was completely under the level of liquid metal, and the entire working surface of the filter was evenly heated by the melt. Since in this scheme the filter is installed inside the melting chamber, optimal conditions for using not only its front, but also the side surface of the filter are provided. It should be emphasized that the ceramic foam filter in this case serves two interrelated purposes. The first is to ensure an increase in the quality of the melted metal. The second is to prevent the connecting channel from becoming overgrown.

In a series of experiments, it was found that the average specific (by mass) efficiency of the circuit's functioning when remelting thin-walled and small aluminium waste was 83% – i.e. from every 1 kg of charge loaded into the circuit, about 830 g of metal passed into the melt. Accordingly, irrecoverable metal losses (primarily waste) did not exceed 17%.

Typically, one beverage can of 500 ml weigh ca. 15 g, of which the actual weight of the aluminium alloy is at least 90%. However, as result of recycling,

metal loss and changing its chemical composition are inevitable. As previously noted, this depends on the method of remelting and its modes, but above all, on the storage conditions of the cans, especially after their use. As a result, the initially identical type of melted charge in different portions may have different contamination with paint coatings, oils, and different degrees of corrosion. Also, if other types of waste (chips, foil, gating system parts, etc.) are added to different portions of the charge for remelting, the final amount, chemical composition and properties of the recycled metal may change significantly.

For presented experiment, changes of the chemical composition of experimental alloy are given in Table 2.

As can be seen from Table 2, after remelting waste portion of 20 kg (it is 25% of the mass of the initial alloy in circuit), the content of such a harmful impurity as Fe increased ca. 30%. It is obvious that this waste portion was heavily contaminated with iron-containing corrosion products.

After melting the scrap charge, samples were taken and cylindrical specimens with a diameter of

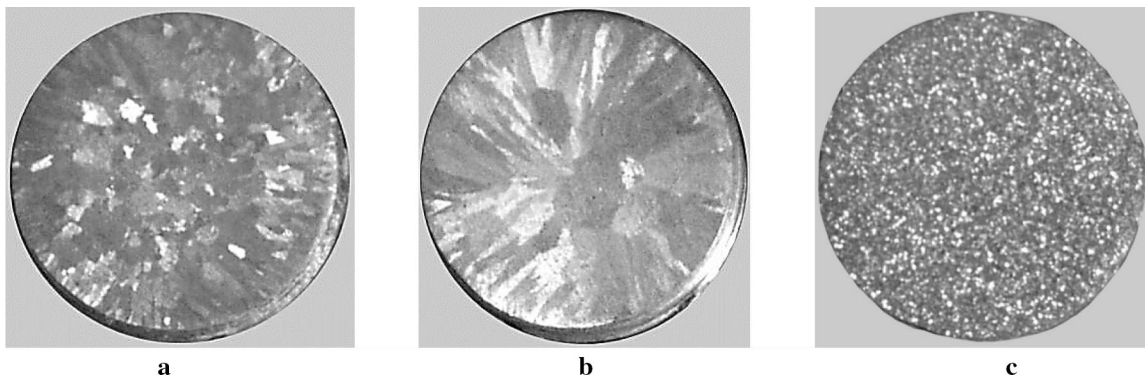


**Figure 11** Effect of filtration on the macrograin size of aluminium cast specimen ( $\varnothing$  15 mm) obtained by remelting thin-walled scrap in experimental melting circulation circuit with MDP: **a**—remelted metal without filtration; **b**—remelted metal filtrated

through ceramic foam filter; **c**—remelted metal filtrated through ceramic foam filter and modified by the ligature (master alloy) AlTi5B1 (Al—base, Ti—5% by weight, B—1% by weight).

15 mm were cast. The transverse macrosections were made. In the first case, there was no filter, in the second case, the melt passed through a ceramic foam filter, and in the third case, the melt obtained after filtering was additionally modified with AlTi5B1 ligature. It is evident that filtering significantly affects the content of non-metallic inclusions. In the second sample, compared to the first one, the average size of the macrograin increased (Fig. 11), which indicates the removal of a significant number of non-metallic inclusions, especially medium and small ones, which are crystallization centres.

### Areas of application

The metal after remelting is subjected certainly to chemical analysis. According to its result, the metal is using as additional charge in the following processes:

- At re-producing an alloy for thin-walled containers or foil;
- At obtaining alloys for castings;
- At manufacturing wrought alloys for stamping metal parts;
- At deoxidation of steel in metallurgical technologies.

The directions for intensifying the proposed process and its industrial testing are as follows:

- (1) The possibility of heating the charge before feeding it into the melt, including directly in the atmosphere of an unheated melting chamber;
- (2) In powerful industrial installations, it is possible to achieve overheating of pure aluminium metal above 750 °C (but not more than 800 °C in order to avoid accelerated oxidation of the melt and its saturation with hydrogen);
- (3) When working not with pure aluminium, but with its alloys, the amount of necessary overheating of the metal entering the unheated chamber is reduced (to values of about 640–650 °C, which is 10–20 °C higher than liquidus temperature  $t_{liq}$  for most aluminium alloys).

### Conclusion

In general, the efficiency of remelting thin-walled aluminium waste depends on the method of transferring thermal energy to the object being remelted.

To reduce the waste of the remelted charge, it is necessary to completely exclude its direct heating and carry out melting in a flow of superheated melt. At the same time, modern technologies for remelting aluminium waste are based on the use of two-chamber systems connected by channels. One of the chambers is heated by a heat source and serves to accumulate the melt; the other is unheated and is intended for remelting the charge in the melt flow coming from the heated chamber. In this case, the circulation of metal in such a system is almost universally carried out using an electromagnetic pump installed on one of the connecting channels.

It seems preferable to use in these systems magnetodynamic pumps designed by PTIMA NAS of Ukraine, which have a higher power factor than running magnetic field pumps, allow for more rational control of the thermal and hydrodynamic parameters of the waste remelting process, expand the capabilities of the technology, especially when refining the deposited melt, and also in emergency situations.

A laboratory experimental MHD circulation circuit has been developed for the effective remelting of thin-walled and small aluminium waste, which includes a magnetodynamic pump.

Mathematical modelling and preliminary calculation of the thermal parameters of the process were carried out. The results of the full-scale experiment confirmed the correctness of the theoretical assumptions made and the high efficiency of the developed MHD circulation melting circuit.

### Acknowledgements

The work was carried out within the framework of the MSCA4Ukraine project funded by the European Union.

In addition, studies were carried out as part of the research work (project) according to competitions of the National Academy of Sciences of Ukraine: III-42-23-721 “Development of the scientific and technological basis of the application of electromagnetic influences in order to increase the efficiency of the process of filtering metal melts from non-metallic inclusions” (UA State reg. no. 0123U100176).

Also, researches were carried out in accordance with the planned R&D work of “TECHNICAL UNIVERSITY “METINVEST POLYTECHNIC” LLC: “Development of scientific and methodological foundations

for improving metallurgical processes, equipment and methods of managing their efficiency” (UA State reg. no. 0123U102947).

### Author contributions

Oleksiy Smirnov contributed to supervision, conceptualization, interpretation, and writing—review and editing. Vladyslav Fikssen contributed to methodology, investigation, data curation, and visualization. Volodymyr Kukhar contributed to conceptualization, validation, visualization, and writing—review and editing. Maksym Goryuk contributed to methodology, validation, visualization, calculations, and writing—original draft. Oleksandr Hrushko contributed to formal analysis, investigation, and writing—review and editing. Oleksandr Rud contributed to data procession, interpretation, and validation. Viktor Lomakin contributed to investigation and data procession.

### Funding

Open access funding provided by Danube University Krems University for Continuing Education.

### Data availability

Data are available upon request.

### Declarations

**Conflict of interest** The authors declare that they have no conflict of interest.

**Ethical approval** Not applicable.

**Open Access** This article is licensed under a Creative Commons Attribution 4.0 International License, which permits use, sharing, adaptation, distribution and reproduction in any medium or format, as long as you give appropriate credit to the original author(s) and the source, provide a link to the Creative Commons licence, and indicate if changes were made. The images or other third party material in this article are included in the article’s Creative Commons

licence, unless indicated otherwise in a credit line to the material. If material is not included in the article’s Creative Commons licence and your intended use is not permitted by statutory regulation or exceeds the permitted use, you will need to obtain permission directly from the copyright holder. To view a copy of this licence, visit <http://creativecommons.org/licenses/by/4.0/>.

### References

- [1] Mahfoud M, Emadi D (2010) Aluminum recycling—challenges and opportunities. *Adv Mat Res* 83–86:571–578. <https://doi.org/10.4028/www.scientific.net/AMR.83-86.571>
- [2] Dragobetskii V, Shapoval A, Naumova E, Shlyk S, Mospan D, Sikulskiy V (2017) The technology of production of a copper–aluminum–copper composite to produce current lead buses of the high–voltage plants. In: 2017 International Conference on Modern Electrical and Energy Systems (MEES), IEEE, Kremenchuk, Ukraine, 2017, pp 400–403. <https://doi.org/10.1109/MEES.2017.8248944>
- [3] Gokelma M, Diaz F, Oner IE, Friedrich B, Tranell G (2020) An assessment of recyclability of used aluminium coffee capsules. In: Tomsett A (ed) *Light Metals 2020. The Minerals, Metals & Materials Series*, Springer, Cham, 2020, pp 1101–1109. [https://doi.org/10.1007/978-3-030-36408-3\\_149](https://doi.org/10.1007/978-3-030-36408-3_149)
- [4] Cui J, Roven HJ (2010) Recycling of automotive aluminum. *Trans Nonferrous Met Soc China* 20(11):2057–2063. [https://doi.org/10.1016/S1003-6326\(09\)60417-9](https://doi.org/10.1016/S1003-6326(09)60417-9)
- [5] Schmitz C (2014) *Handbook of aluminium recycling: mechanical preparation, metallurgical processing, heat treatment*, 2nd edn. Vulkan Verlag, Essen, Germany, p 538
- [6] Smil V (2023) *Materials and dematerialization: making the modern world*, 2nd edn. John Wiley & Sons, New York
- [7] AlSaffar KA, Bdeir LMH (2008) Recycling of aluminum beverage cans. *Journal of Engineering and Development* 12(3):157–163. <https://www.iasj.net/iasj/pdf/295df61f1db3965a>
- [8] Gaustad G, Olivetti E, Kirchain R (2012) Improving aluminum recycling: a survey of sorting and impurity removal technologies. *Resour Conserv Recycl* 58:79–87. <https://doi.org/10.1016/j.resconrec.2011.10.010>
- [9] Hatayama H, Daigo I, Matsuno Y, Adachi Y (2009) Assessment of the recycling potential of aluminum in Japan, the United States. *Eur China Mater Trans* 50(3):650–656. <https://doi.org/10.2320/matertrans.MRA2008337>

- [10] Ozer G, Burgucu S, Marsoglu M (2012) A study on the recycling of aluminium alloy 7075 scrap. *Mater Test* 54(3):175–178. <https://doi.org/10.3139/120.110309>
- [11] Lin R, Liu B, Zhang J, Zhang S (2022) Microstructure evolution and properties of 7075 aluminum alloy recycled from scrap aircraft aluminum alloys. *J Market Res* 19:354–367. <https://doi.org/10.1016/j.jmrt.2022.05.011>
- [12] Zhou B, Liu B, Zhang S, Lin R, Jiang Y, Lan X (2021) Microstructure evolution of recycled 7075 aluminum alloy and its mechanical and corrosion properties. *J Alloy Compd* 879:160407. <https://doi.org/10.1016/j.jallcom.2021.160407>
- [13] Ahmad F, Akhyar A, Masri A (2019) Experiment on hardness and impact strength of recycled aluminum alloys by metal casting process. *Mater Sci Forum* 961:65–72. <https://doi.org/10.4028/www.scientific.net/MSF.961.65>
- [14] Odusote JK, Ajayi PA (2016) Mechanical properties and microstructure of recycled aluminum cast with zinc and copper additions. *Int J Metalcast* 10(4):483–490. <https://doi.org/10.1007/s40962-016-0060-4>
- [15] Tillova E, Chalupova M, Borko K, Kucharikova L (2016) Changes of fracture surface in recycled A356 cast alloy. *Mater Today Proc* 3(4):1183–1188. <https://doi.org/10.1016/j.matpr.2016.03.009>
- [16] Widyantoro DD, Fatriansyah JF, Firmansyah MR, Prasetyo Y (2019) Removal of oxide inclusions in aluminium scrap casting process with sodium based fluxes. *MATEC Web Conf* 269:07002. <https://doi.org/10.1051/mateconf/201926907002>
- [17] Kumar EK, Patel SS, Panda SK, Patle BK, Makki E, Giri J (2024) A comprehensive exploration of shape memory alloys: Fundamentals, structural reinforcements, nano-analysis, machine learning perspective, and emerging applications. *Mech Adv Mater Struc* 2024:1–34. <https://doi.org/10.1080/15376494.2024.2307471>
- [18] Anishchenko A, Kukhar V, Artiukh V, Arkhipova O (2018) Formulas for description of shells superplastic forming. *MATEC Web Conf* 239:06007. <https://doi.org/10.1051/mateconf/201823906007>
- [19] Kucharikova L, Tillova E, Bokuvka O (2016) Recycling and properties of recycled aluminium alloys used in the transportation industry. *Transport Problems* 11(2):117–122. <https://doi.org/10.20858/tp.2016.11.2.11>
- [20] Das SK, Green JAS, Kaufman JG, Emadi D, Mahfoud M (2010) Aluminum recycling—an integrated, industry wide approach. *JOM* 62(2):23–26. <https://doi.org/10.1007/s11837-010-0026-6>
- [21] Smirnov OM, Rud OD, Fikssen VN, Skorobagatko YuP, Monastyrskaya TO, Goryuk MS, Semenko AY, Yashchenko OV (2023) Impact of MHD-processing on technological properties of high-strength casting Al–Cu alloys. *Metallofiz Noveishie Tekhnol* 45(9):1125–1139. <https://doi.org/10.15407/mfint.45.09.1125>
- [22] Xiao Y, Reuter M, Vonk P, Vonken J, Orbon H, Probst Th, Boin U (2000) Experimental study on aluminum scrap recycling. In: Stewart Jr DR, Daley JC, Stephens RL (eds) *Fourth International Symposium on Recycling of Metals and Engineered Materials*. TMS (The Minerals, Metals & Materials Society), 2000, pp 1075–1087. <https://doi.org/10.1002/9781118788073.ch93>
- [23] Bourgeois L, Dwyer C, Weyland M, Nie J-F, Muddle BC (2012) The magic thicknesses of  $\theta'$  precipitates in Sn-microalloyed Al–Cu. *Acta Mater* 60(2):633–644. <https://doi.org/10.1016/j.actamat.2011.10.015>
- [24] Verran GO, Kurzawa U (2008) An experimental study of aluminum can recycling using fusion in induction furnace. *Resour Conserv Recy* 52(5):731–736. <https://doi.org/10.1016/j.resconrec.2007.10.001>
- [25] Das SK (2006) Emerging trends in aluminum recycling: reasons and responses. In: Galloway TJ (ed) *Light Metals 2006*. The Minerals, Metals & Materials Society, San Antonio, Texas, USA, 2006, pp 911–916. <https://secat.net/wp-content/uploads/Emerging-Trends-in-Aluminum-Recycling-Reasons-and-Responses.pdf>
- [26] Kevorkijan V (2013) Modeling of alternative compositions of recycled wrought aluminum alloys. *JOM* 65(8):973–981. <https://doi.org/10.1007/s11837-013-0669-1>
- [27] Holzschuh GG, Moraes JAR, Garcia SB, Zanesco I, Kipper LM, Schneider RCS (2023) Casting of recycled aluminum cans to electrical conductivity tape production. *J Waste Manag Recycl Technol* 1(2):1–7. [https://doi.org/10.47363/JWMRT/2023\(1\)106](https://doi.org/10.47363/JWMRT/2023(1)106)
- [28] Ozer G, Yuksel C, Comert ZY, Guler KA (2013) The effects of process parameters on the recycling efficiency of used aluminium beverage cans (UBCs). *Mater Test* 55(5):396–400. <https://doi.org/10.3139/120.110448>
- [29] Karnaukh SG, Markov OE, Alieva LI, Kukhar VV (2020) Designing and researching of the equipment for cutting by breaking of rolled stock. *Int J Adv Manuf Technol* 109:2457–2464. <https://doi.org/10.1007/s00170-020-05824-7>
- [30] Wang Z, Yu Y, Jin Y, Li Z, Sun S, Xu H, Wu C, Zhang D (2022) Solid state recycling of used aluminum alloy beverage cans by thermomechanical consolidation. *Heat Treat Surf Eng* 4(1):90–98. <https://doi.org/10.1080/25787616.2022.2158562>
- [31] Rosandi Y, Urbassek HM (2013) Melting of Al by ultrafast laser pulses: dynamics at the melting threshold. *Appl Phys A* 110:649–654. <https://doi.org/10.1007/s00339-012-7145-6>

- [32] Ahmed A, Majeed A, Atta Z, Jia G (2019) Dimensional quality and distortion analysis of thin-walled alloy parts of AlSi10Mg manufactured by selective laser melting. *J Manuf Mater Process* 3(2):51. <https://doi.org/10.3390/jmmp3020051>
- [33] Hrudkina NS, Markov OE, Shapoval AA, Titov VA, Aliiev IS, Abhari P, Malii KV (2021) Mathematical and computer simulation for the appearance of dimple defect by cold combined extrusion. *FME Trans* 50(1):90–98. <https://doi.org/10.5937/fme2201090H>
- [34] Haase M, Tekkaya AE (2014) Recycling of aluminum chips by hot extrusion with subsequent cold extrusion. *Procedia Eng* 81:652–657. <https://doi.org/10.1016/j.proeng.2014.10.055>
- [35] Kokoszka P, Milenin A (2023) The impact of temperature conditions on the manufacturing process and mechanical behavior of beverage can ends during operation. *Materials* 16(18):6137. <https://doi.org/10.3390/ma16186137>
- [36] Wędrychowicz P, Kustra P, Milenin A (2023) A numerical and experimental analysis of the mechanical behavior of the aluminum beverage can with internal varnish layers during axial load force testing. *Materials* 16(19):6603. <https://doi.org/10.3390/ma16196603>
- [37] Göknelma M, Aarnæs TS, Maier J, Friedrich B, Tranell G (2019) Behaviour of aluminium carbide in al-melts during re-melting. In: Chesonis C (ed) *Light Metals 2019*. Springer International Publishing, Cham, pp 1033–1039. [https://doi.org/10.1007/978-3-030-05864-7\\_126](https://doi.org/10.1007/978-3-030-05864-7_126)
- [38] Risonarta VY, Anggono J, Suhendra YM, Nugrowibowo S, Jani Y (2019) Strategy to improve recycling yield of aluminium cans. *E3S Web Conf* 130:01033. <https://doi.org/10.1051/e3sconf/201913001033>
- [39] Khrebtova O, Shapoval O, Markov O, Kukhar V, Hrudkina N, Rudych M (2022) Control systems for the temperature field during drawing, taking into account the dynamic modes of the technological installation. In: 2022 IEEE 4th International Conference on Modern Electrical and Energy System (MEES), IEEE, Kremenchuk, Ukraine, 2022, pp 1–6. <https://doi.org/10.1109/MEES58014.2022.10005724>
- [40] Palacz M, Melka B, Wecki B et al (2020) Experimental analysis of the aluminium melting process in industrial cold crucible furnaces. *Met Mater Int* 26:695–707. <https://doi.org/10.1007/s12540-019-00368-2>
- [41] Rot D, Kozeny J, Jirinec S, Jirinec J, Podhrazky A, Poznyak I (2017) Induction melting of aluminium oxide in the cold crucible. In: 2017 18th International Scientific Conference on Electric Power Engineering (EPE), IEEE, Kouty nad Desnou, Czech Republic, 2017, pp 1–4. <https://doi.org/10.1109/EPE.2017.7967281>
- [42] Chamorro X, Herrero-Dorca N, Bernal D, Hurtado I (2019) Induction skull melting of Ti-6Al-4V: process control and efficiency optimization. *Metals* 9:539. <https://doi.org/10.3390/met9050539>
- [43] Rader D, Schmitz W, Dahmen C, Uerlichs P, Mertens T (2023) Recycling organically contaminated aluminum scrap and decarbonization concepts. *Heat Process* 2:61–68
- [44] Steglich J, Dittrich R, Rosefort M, Friedrich B (2016) Pre-treatment of beverage can scrap to increase recycling efficiency. *J Mater Sci Eng A* 3(3–4):57–65. <https://doi.org/10.17265/2161-6213/2016.3-4.003>
- [45] Raabe D, Ponge D, Uggowitzer P, Roscher M, Paolantonio M et al (2022) Making sustainable aluminum by recycling scrap: the science of “dirty” alloys. *Prog Mater Sci* 128:100947. <https://doi.org/10.1016/j.pmatsci.2022.100947>
- [46] Grab HW, Migchielsen JM (2008) New developments in the design of twin chamber aluminium melting furnaces. *World Metall Erzmetall* 61(2):104–108
- [47] Wibner S, Antrekowitsch H, Falkensammer B (2020) Representative sampling, fractionation and melting of Al-scrap. In: Tomsett A (ed) *Light metals 2020*. The minerals, metals & materials series. Springer International Publishing, Cham, pp 1083–1090. [https://doi.org/10.1007/978-3-030-36408-3\\_147](https://doi.org/10.1007/978-3-030-36408-3_147)
- [48] Smirnov O, Skorobagatko Yu, Goryuk M, Voron M, Semenko A, Hoida D, Semiryagin S (2023) Influence of combined vibration with cavitation and electromagnetic impact on the cast aluminium alloy grain refining. *Metallofiz Noveishie Tekhnol* 45(7):883–900. <https://doi.org/10.15407/mfint.45.07.0883>
- [49] Fritzsche R, Grayson J (2019) Electromagnetic transfer and circulation (ETAC) of molten aluminum metal and its alloys. In: Chesonis C (ed) *Light Metals 2019*. The minerals, metals & materials series. Springer International Publishing, Cham, pp 1173–1178. [https://doi.org/10.1007/978-3-030-05864-7\\_144](https://doi.org/10.1007/978-3-030-05864-7_144)
- [50] Pavlovs S, Jakovičs A, Baake E, Nacke B, Kirpo M (2011) LES modelling of turbulent flow, heat exchange and particle transport in industrial induction channel furnaces. *Magnetohydrodynamics* 47(4):399–412
- [51] Vives C, Ricou R (1991) Magnetohydrodynamic flows in a channel-induction furnace. *Metall Trans B* 22:193–209. <https://doi.org/10.1007/BF02652484>
- [52] Grayson J (2014) Forced circulation can improve furnace performance and efficiency. *Alum Int Today* 26(3):25–26
- [53] Rader KE, Sabau AS, Rohatgi A (2023) Microstructural refinement in ultrasonically modified A356 aluminum castings. *J Mater Sci* 58:17340–17361. <https://doi.org/10.1007/s10853-023-08999-y>

- [54] Smirnov OM, Narivskiy AV, Smirnov EN, Verzilov AP, Semenko AYU, Goryuk MS (2021) Development of a two-chamber MHD tundish for metal casting. *Sci Innov* 17(4):19–24. <https://doi.org/10.15407/scine17.04.019>
- [55] Smirnov OM, Narivskiy AV, Smirnov EN, Semenko AYU, Verzilov OP (2021) Increasing the dosing accuracy of magnetodynamic foundry equipment. *Sci Innov* 17(5):42–49. <https://doi.org/10.15407/scine17.05.042>
- [56] Dubodelov V, Fikssen V, Slazhniev M, Goryuk M, Skorobagatko Iu, Seredenko E, Yashchenko O (2015) Modernization of casting magnetodynamic equipment. In: Proceedings of the 8th International Conference on Electromagnetic Processing of Materials (EPM 2015), Cannes, France, 2015, pp 601–604. <https://hal.science/hal-01336201/document>
- [57] Vallejo-Olivares A, Gertjegerdes T, Høgåsen S, Friedrich B (2024) Tranell G (2024) Effects of compaction and thermal pre-treatments on generation of dross and off-gases in aluminium recycling. *J Sustain Metall* 10:69–82. <https://doi.org/10.1007/s40831-023-00773-3>
- [58] Steglich J, Friedrich B, Rosefort M (2020) Dross formation in aluminum melts during the charging of beverage can scrap bales with different densities using various thermal pretreatments. *JOM* 72(10):3383–3392. <https://doi.org/10.1007/s11837-020-04268-4>
- [59] Steglich J, Dittrich R, Rombach G, Rosefort M, Friedrich B, Pichat A (2017) Dross formation mechanisms of thermally pre-treated used beverage can scrap bales with different density. In: Ratvik AP (ed) *Light Metals 2017. The Minerals, Metals & Materials Series*. Springer International Publishing, Cham, pp 1105–1113. [https://doi.org/10.1007/978-3-319-51541-0\\_133](https://doi.org/10.1007/978-3-319-51541-0_133)
- [60] Dittrich R, Friedrich B, Rombach G, Steglich J, Pichat A (2017) Understanding of interactions between pyrolysis gases and liquid aluminum and their impact on dross formation. In: Ratvik AP (ed) *Light Metals 2017. The minerals, metals & materials series*. Springer International Publishing, Cham, pp 1457–1464. [https://doi.org/10.1007/978-3-319-51541-0\\_174](https://doi.org/10.1007/978-3-319-51541-0_174)
- [61] Kakac S, Yener Y, Naveira-Cotta CP (2018) *Heat Conduction*, 5th edn, CRC Press, Boca Raton. <https://doi.org/10.1201/b22157>
- [62] Hahn DW, Ozisik MN (2012) *Heat conduction*, 3rd edn. John Wiley & Sons
- [63] The Engineering ToolBox (2003). Surface Emissivity Coefficients. [online] Available at: [https://www.engineeringtoolbox.com/emissivity-coefficients-d\\_447.html](https://www.engineeringtoolbox.com/emissivity-coefficients-d_447.html)
- [64] Wen CD, Mudawar I (2005) Emissivity characteristics of polished aluminum alloy surfaces and assessment of multispectral radiation thermometry (MRT) emissivity models. *Int J Heat Mass Tran* 48(7):1316–1329. <https://doi.org/10.1016/j.ijheatmasstransfer.2004.10.003>
- [65] Reddy PC, Raju MC, Raju GSS (2015) Magneto hydrodynamic convective double diffusive laminar boundary layer flow past an accelerated vertical plate. *Int J Eng Res Afr* 20:80–92. <https://doi.org/10.4028/www.scientific.net/jera.20.80>
- [66] Leitner M, Leitner T, Schmon A et al (2017) Thermophysical properties of liquid aluminum. *Metall Mater Trans A* 48:3036–3045. <https://doi.org/10.1007/s11661-017-4053-6>
- [67] Assael MJ, Kakosimos K, Banish RM et al (2006) Reference data for the density and viscosity of liquid aluminum and liquid iron. *J Phys Chem Ref Data* 35(1):285–300. <https://doi.org/10.1063/1.2149380>
- [68] Chabak Y, Efremenko B, Petryshynets I et al (2021) Structural and tribological assessment of biomedical 316 stainless steel subjected to pulsed-plasma surface modification: comparison of LPBF 3D printing and conventional fabrication. *Materials* 14:7671. <https://doi.org/10.3390/ma14247671>
- [69] Duriagina Z, Kulyk V, Kovbasiuk T, Vasylyv B, Kostyryzh A (2021) Synthesis of functional surface layers on stainless steels by laser alloying. *Metals* 11(3):434. <https://doi.org/10.3390/met11030434>
- [70] Zhang Y, Li Q, Zhou H (2016) *Theory and calculation of heat transfer in furnaces*, 1st edn. Elsevier. <https://doi.org/10.1016/C2013-0-13233-3>

**Publisher's Note** Springer Nature remains neutral with regard to jurisdictional claims in published maps and institutional affiliations.